

Multimodel ensemble simulations of present-day and near-future tropospheric ozone

D. S. Stevenson,¹ F. J. Dentener,² M. G. Schultz,³ K. Ellingsen,⁴ T. P. C. van Noije,⁵ O. Wild,^{6,7} G. Zeng,⁸ M. Amann,⁹ C. S. Atherton,¹⁰ N. Bell,¹¹ D. J. Bergmann,¹⁰ I. Bey,¹² T. Butler,¹³ J. Cofala,⁹ W. J. Collins,¹⁴ R. G. Derwent,¹⁵ R. M. Doherty,¹ J. Drevet,¹² H. J. Eskes,⁵ A. M. Fiore,¹⁶ M. Gauss,⁴ D. A. Hauglustaine,¹⁷ L. W. Horowitz,¹⁶ I. S. A. Isaksen,⁴ M. C. Krol,² J.-F. Lamarque,¹⁸ M. G. Lawrence,¹³ V. Montanaro,¹⁹ J.-F. Müller,²⁰ G. Pitari,¹⁹ M. J. Prather,²¹ J. A. Pyle,⁸ S. Rast,³ J. M. Rodriguez,^{22,23} M. G. Sanderson,¹⁴ N. H. Savage,⁸ D. T. Shindell,¹¹ S. E. Strahan,²² K. Sudo,⁶ and S. Szopa¹⁷

Received 9 June 2005; revised 14 October 2005; accepted 19 December 2005; published 26 April 2006.

[1] Global tropospheric ozone distributions, budgets, and radiative forcings from an ensemble of 26 state-of-the-art atmospheric chemistry models have been intercompared and synthesized as part of a wider study into both the air quality and climate roles of ozone. Results from three 2030 emissions scenarios, broadly representing “optimistic,” “likely,” and “pessimistic” options, are compared to a base year 2000 simulation. This base case realistically represents the current global distribution of tropospheric ozone. A further set of simulations considers the influence of climate change over the same time period by forcing the central emissions scenario with a surface warming of around 0.7K. The use of a large multimodel ensemble allows us to identify key areas of uncertainty and improves the robustness of the results. Ensemble mean changes in tropospheric ozone burden between 2000 and 2030 for the 3 scenarios range from a 5% decrease, through a 6% increase, to a 15% increase. The intermodel uncertainty (± 1 standard deviation) associated with these values is about $\pm 25\%$. Model outliers have no significant influence on the ensemble mean results. Combining ozone and methane changes, the three scenarios produce radiative forcings of -50 , 180 , and 300 mW m^{-2} , compared to a CO_2 forcing over the same time period of $800\text{--}1100 \text{ mW m}^{-2}$. These values indicate the importance of air pollution emissions in short- to medium-term climate forcing and the potential for stringent/lax control measures to improve/worsen future climate forcing. The model sensitivity of ozone to imposed climate change varies between models but modulates zonal mean mixing ratios by ± 5 ppbv via a variety of feedback mechanisms, in particular those involving water vapor and stratosphere-troposphere exchange. This level of climate change also reduces the methane lifetime by around 4%. The ensemble mean year 2000 tropospheric ozone budget indicates chemical production, chemical destruction, dry

¹School of Geosciences, University of Edinburgh, Edinburgh, UK.

²Joint Research Centre, Institute for Environment and Sustainability, Ispra, Italy.

³Max Planck Institute for Meteorology, Hamburg, Germany.

⁴Department of Geosciences, University of Oslo, Oslo, Norway.

⁵Atmospheric Composition Research, Royal Netherlands Meteorological Institute, De Bilt, Netherlands.

⁶Frontier Research Center for Global Change, Japan Marine Science and Technology Center, Yokohama, Japan.

⁷Now at Centre for Atmospheric Science, University of Cambridge, Cambridge, UK.

⁸Centre for Atmospheric Science, University of Cambridge, Cambridge, UK.

⁹International Institute for Applied Systems Analysis, Laxenburg, Austria.

¹⁰Atmospheric Science Division, Lawrence Livermore National Laboratory, Livermore, California, USA.

¹¹NASA Goddard Institute for Space Studies, New York, New York, USA.

¹²Ecole Polytechnique Fédérale de Lausanne, Lausanne, Switzerland.

¹³Max Planck Institute for Chemistry, Mainz, Germany.

¹⁴Hadley Centre for Climate Prediction and Research, Met Office, Exeter, UK.

¹⁵rdscientific, Newbury, Berkshire, UK.

¹⁶Geophysical Fluid Dynamics Laboratory, NOAA, Princeton, New Jersey, USA.

¹⁷Laboratoire des Sciences du Climat et de l'Environnement, Gif-sur-Yvette, France.

¹⁸Atmospheric Chemistry Division, National Center of Atmospheric Research, Boulder, Colorado, USA.

¹⁹Dipartimento di Fisica, Università L'Aquila, L'Aquila, Italy.

²⁰Belgian Institute for Space Aeronomy, Brussels, Belgium.

²¹Department of Earth System Science, University of California, Irvine, California, USA.

²²Rosentiel School of Marine and Atmospheric Sciences, University of Miami, Miami, Florida, USA.

²³NASA Goddard Space Flight Center, Greenbelt, Maryland, USA.

deposition and stratospheric input fluxes of 5100, 4650, 1000, and 550 Tg(O₃) yr⁻¹, respectively. These values are significantly different to the mean budget documented by the Intergovernmental Panel on Climate Change (IPCC) Third Assessment Report (TAR). The mean ozone burden (340 Tg(O₃)) is 10% larger than the IPCC TAR estimate, while the mean ozone lifetime (22 days) is 10% shorter. Results from individual models show a correlation between ozone burden and lifetime, and each model's ozone burden and lifetime respond in similar ways across the emissions scenarios. The response to climate change is much less consistent. Models show more variability in the tropics compared to midlatitudes. Some of the most uncertain areas of the models include treatments of deep tropical convection, including lightning NO_x production; isoprene emissions from vegetation and isoprene's degradation chemistry; stratosphere-troposphere exchange; biomass burning; and water vapor concentrations.

Citation: Stevenson, D. S., et al. (2006), Multimodel ensemble simulations of present-day and near-future tropospheric ozone, *J. Geophys. Res.*, *111*, D08301, doi:10.1029/2005JD006338.

1. Introduction

[2] The global environmental issues of climate change and air pollution are closely linked, not least by the trace gas ozone (O₃). Ozone concentrations in the troposphere are thought to have increased significantly since preindustrial times, as a direct result of human activities [Volz and Kley, 1988; Staehelin et al., 1994; Lamarque et al., 2005a]. Tropospheric O₃ increases represent the third largest greenhouse gas contribution to radiative forcing of climate change over this time period, with a forcing equivalent to about 24% of that from carbon dioxide [Ramaswamy et al., 2001]. Ozone is also a serious and ubiquitous air pollutant, affecting the respiratory health of a large proportion of the world population [World Health Organization, 2003], reducing the yields of staple agricultural crops such as wheat and soy bean, and damaging natural ecosystems [Emberson et al., 2003; Wang and Mauzerall, 2004].

[3] There are two sources of tropospheric ozone: transport from the stratosphere, and in situ chemical production. Ozone production takes place when carbon monoxide (CO) and hydrocarbons are photo-oxidized in the presence of nitrogen oxides (NO_x = NO + NO₂) [Crutzen, 1974; Liu et al., 1980; Atkinson, 2000]. The ozone budget is closed by two loss processes: dry deposition to the Earth's surface, and chemical destruction. Ozone destruction occurs mainly via reactions with water vapor (following photolysis) and with hydrogen peroxy and hydroxyl radicals (HO_x = HO₂ + OH). Integrated over the whole troposphere, chemical production and loss rates are several times larger than the influx from the stratosphere and the surface deposition flux.

[4] The main ozone precursors (CO, hydrocarbons, and NO_x) are all emitted as by-products of human activities, as well as having significant natural sources. The same anthropogenic and natural emissions also influence HO_x, affecting ozone destruction. The rapid growth in anthropogenic emissions following industrialization has been the major driver of increases in tropospheric ozone, and has been the subject of intensive study [e.g., Levy et al., 1985; Crutzen and Zimmerman, 1991; Lelieveld and Dentener, 2000; Lamarque et al., 2005a]. Interest has more recently turned to the potential influence of climate change on future levels of ozone [Johnson et al., 1999, 2001; Isaksen et al., 2003; Grenfell et al., 2003; Stevenson et al., 2005; Hauglustaine et al., Murazaki and Hess, 2006].

Warming will increase water vapor concentrations, and changes in temperature and water vapor will affect the reaction rates of many chemical conversions. Climate change may also alter global circulation dynamics, changing several processes that govern the distribution of tropospheric ozone, such as stratosphere-troposphere exchange, the distribution of convection, and ventilation of the boundary layer. Changes in climate will also affect many of the natural sources of trace gases, such as wetland CH₄ [Walter and Heimann, 2000; Gedney et al., 2004; Shindell et al., 2004], biogenic volatile organic compounds [Sanderson et al., 2003; Wiedinmyer et al., 2005; Lathière et al., 2005], lightning NO_x [Price et al., 1997] and soil NO_x [Ganzeveld et al., 2002].

[5] Global atmospheric chemistry models currently provide our best estimates of tropospheric distributions of trace species such as ozone and the hydroxyl radical (OH). These models underpin our understanding of the oxidizing capacity of the atmosphere, and radiative forcings arising from changes to methane (CH₄) and O₃ concentrations [e.g., Prather et al., 2001, 2003; Gauss et al., 2003]. As such, they constitute the best tools at our disposal for making quantitative future projections of tropospheric composition.

[6] Such models are only approximations of the real atmosphere, and exhibit uncertainties arising from many processes, including emissions, transport (resolved advection and subgrid-scale convection), chemistry (photochemical, gas phase, aqueous phase, and heterogeneous reactions), mixing, deposition, and also from upper and lower boundary conditions. All these processes are interrelated, and tend to be handled by specific models in different ways. Consequently, models show a range of sensitivities to changes in, for example, future trace gas emissions and climate.

[7] Some previous model intercomparison studies have focused on comparisons of models and measurements [e.g., Brunner et al., 2003, 2005; Roelofs et al., 2003; Kinne et al., 2005; Textor et al., 2005], but this is not the main thrust of the work presented here. Instead, this paper intercompares and synthesizes simulated ozone results from a wide cross section of state-of-the-art models, and is part of a larger study [Dentener et al., 2006a] coordinated by the European Union project Atmospheric Composition Change: the European Network of excellence (ACCENT; <http://www.accent-network.org>). The use of a wide range of

differently formulated models allows us to increase the robustness of future projections, and quantify levels of uncertainty. Other aspects of this wider modeling study include a detailed analysis of surface ozone, including impacts on human health and vegetation (K. Ellingsen et al., Ozone air quality in 2030: A multi-model assessment of risks for health and vegetation, manuscript in preparation, 2006); a comparison of modeled NO₂ tropospheric columns with satellite observations [van Noije et al., 2006]; a comparison of modeled and measured CO (D. Shindell et al., Multi-model simulations of carbon monoxide: Comparison with observations and projected near-future changes, submitted to *Journal of Geophysical Research*, 2006, hereinafter referred to as Shindell et al., submitted manuscript, 2006); and an analysis of simulated deposition budgets of NO_y, SO_x, and NH_x (F. Dentener et al., Nitrogen and sulfur deposition on regional and global scales: A multimodel evaluation, submitted to *Global Biogeochemical Cycles*, 2005, hereinafter referred to as Dentener et al., submitted manuscript, 2005). A parallel study [Gauss et al., 2005] intercompares ozone from a similar range of models from preindustrial to present day, with a particular focus on both tropospheric and stratospheric changes.

[8] In the following section, we briefly describe some of the pertinent features of the participating models, emphasizing potentially important differences in their formulation. In section 3, we describe the model simulations that were carried out, before reporting and discussing results in section 4. Section 4 firstly describes how we have processed results from a diverse range of models, and created ensemble means and standard deviations. Ozone results for the year 2000 are then described and compared to ozonesonde observations. We then consider results from the 2030 scenarios, in terms of changes in both emissions and climate relative to 2000. We present tropospheric ozone budgets and methane lifetimes, and calculate radiative forcings for the various cases. The last section presents a summary and conclusions.

2. Participating Models: Sources of Differences

[9] Results from a total of 26 different models (see Appendix A and Table A1) are analyzed here. These 26 models include some cases where the same “core” model was used in two or more different configurations; e.g., the models CHASER, GMI, LMDz/INCA and MATCH-MPIC were driven by a variety of different underlying meteorological fields. Nearly all the models were set up as chemistry-transport models (CTMs); in these models the meteorology is not influenced by the chemical fields. Only two models (CHASER_GCM and ULAQ) were set up as fully coupled chemistry-climate models (CCMs), where the chemical fields enter the radiation calculations of the driving general circulation model (GCM), and directly influence the dynamics. For ULAQ, this fully coupled mode was only switched on for the climate change simulation (S5; simulations are described in section 3). Of the CTMs, thirteen were driven by numerical weather prediction (NWP) data, with nine using European Centre for Medium-Range Weather Forecasts (ECMWF) analyses or forecasts. The other thirteen models were driven by GCM output, with eleven different drivers. Ms. Of these models, ten

simulated the climate change scenario. When available, each of the 26 model results is given equal weight in the following analysis. We also check for the potential influence of model outliers on our conclusions.

[10] Global horizontal resolution ranged from 10° × 22.5° (ULAQ) to 1.9° × 1.9° (MOZECH, MOZ2-GFDL), with one model (TM5) operating a 1° × 1° nested grid over Europe, North America and Asia. The number of vertical levels ranged from 9 (STOCHEM_HadAM3) to 60 (MATCH models), with typically 20 levels of variable thickness in the troposphere, increasing in resolution toward the surface. The lowest layer depth ranged from about 35 to 800 m. Studies have shown that, all other things being equal, higher-resolution models tend to produce less ozone from the same levels of precursor emissions, due to the lower levels of forced “mixing” generated when emissions are added to large grid boxes [e.g., Liang and Jacobsen, 2000; Esler, 2003]. We might therefore expect the lower-resolution models to be inherently more mixed and hence more chemically active than the higher-resolution models.

[11] The cross-tropopause flux of ozone [Gettelman et al., 1997; Roelofs et al., 2003; Olsen et al., 2004] is a key determinant of upper tropospheric ozone concentrations. Models used a wide variety of upper boundary conditions. Two models (LLNL-IMPACT and ULAQ) included detailed stratospheric chemistry. The UIO_CTM2 model used stratospheric profiles from an earlier run with full stratospheric chemistry. The FRSGC/UCI model used the “linearized ozone chemistry” (LINOZ) scheme [McLinden et al., 2000], which can be considered a simplified stratospheric chemistry scheme. Some models employed “prescribed flux” methods: GEOS-CHEM and GMI used the “synthetic ozone” (SYNOZ) scheme [McLinden et al., 2000]. STOCHEM-HadAM3 added an ozone flux at 100 hPa, calculated from an ozone climatology and the local vertical winds. Other models fixed ozone concentrations above a certain level: p-TOMCAT (<10 hPa); UM_CAM, MATCH-MPIC (<30 hPa); IASB (<50 hPa); and GISS (above tropopause). Another method used was to relax or nudge toward a climatology above a certain level: CHASER, TM5 (<50 hPa); LMDz/INCA (>380 K isentrope; <~100 hPa); TM4 (<60 hPa (30°S–30°N); <123 hPa elsewhere); and STOCHEM_HadGEM (above tropopause). Finally, some models used a combination of fixed ozone above a certain level and relaxation below this level: MOZ2-GFDL (fixed <14 hPa, relax between 14 hPa and tropopause), MOZECH and MOZECH2 (fixed <30 hPa, relax <100 hPa in the tropics and <200 hPa in the extratropics), MOZART4 (fixed <50 hPa, relax between 50 hPa and tropopause). A relaxation e-folding timescale of 3–10 days is typically applied. The relative merits of these different schemes are not well known, but some of these variants have been compared in the consistent framework of ERA-40 (45-year ECMWF reanalysis [Simmons and Gibson, 2000]) by van Noije et al. [2004].

[12] Deposition of ozone to the Earth’s surface and biosphere strongly influences boundary layer ozone concentrations. Models used deposition schemes of varying levels of sophistication, but all used “resistance” type formulations [e.g., Wesely, 1989] coupled to prescribed land cover distributions. Inspection of ozone deposition distri-

Table 1. Specifications of the Simulations^a

Code	Name	Meteorology	Emissions	Reference
S1	Y2000	2000/1995–2004	2000 (EDGAR3.2)	<i>Olivier and Berdowski</i> [2001]
S2	CLE	2000/1995–2004	2030 IIASA CLE	<i>Dentener et al.</i> [2005]
S3	MFR	2000/1995–2004	2030 IIASA MFR	<i>Dentener et al.</i> [2005]
S4	A2	2000/1995–2004	2030 SRES A2	<i>Nakicenovic et al.</i> [2000]
S5	CLE-AC	2025–2034	2030 IIASA CLE	<i>Stevenson et al.</i> [2005]

^aThe code and the name are used interchangeably in the text.

butions from the models suggest that the schemes generate quite variable deposition velocities over different terrains, although global deposition fluxes are relatively consistent (see budget analysis below).

[13] Convective mixing of ozone and its precursors exerts a major control on the vertical distribution of tropospheric ozone [*Lelieveld and Crutzen*, 1994; *Lawrence et al.*, 2003; *Olivier et al.*, 2004; *Doherty et al.*, 2005]. All models include parametrizations for convection; the most commonly used (by seven of the models) is the mass flux scheme of *Tiedtke* [1989], sometimes with modifications. Some model convection schemes are tuned using vertical profiles of the short-lived isotope ²²²Rn [e.g., *Jacob et al.*, 1997; *Rasch et al.*, 2000]; however, observations of ²²²Rn are sparse, and soil emissions are not well known [e.g., *Robertson et al.*, 2005]. In addition, convection over oceanic areas is essentially not considered, as the ²²²Rn source is land-based. Consequently, convection schemes are poorly constrained, and are probably a major source of differences between models. Model uncertainties associated with convection may be exacerbated because convection is often colocated with lightning and tropical vegetation, key natural sources of the ozone precursors NO_x and isoprene (C₅H₈). Convective mixing promotes interaction between these two sources throughout the depth of the tropical troposphere, with potentially important implications for ozone [e.g., *von Kuhlmann et al.*, 2004; *Doherty et al.*, 2005]. Model uncertainties associated with convection also include wash-out of key species (e.g., nitric acid, HNO₃, and hydrogen peroxide, H₂O₂) [e.g., *Sudo and Takahashi*, 2001].

[14] Chemical schemes continue to develop in complexity through the addition and expansion of nonmethane hydrocarbon (NMHC) schemes [e.g., *Houweling et al.*, 1998; *Wang et al.*, 1998; *Collins et al.*, 1999; *Roelofs and Lelieveld*, 2000; *von Kuhlmann et al.*, 2003a], and the inclusion of aerosol modules, allowing gas-aerosol interactions [e.g., *Tie et al.*, 2001, 2003; *Martin et al.*, 2003; *Bauer et al.*, 2004; *Bell et al.*, 2005]. All the models include some description of NMHC chemistry, but they range from relatively highly parameterized “lumped” schemes (e.g., GISS: 35 species) to more detailed schemes (e.g., MOZART4: 96 species). Isoprene degradation schemes in the models show a similar range of complexity, and this may account for some variations in tropical ozone [e.g., *Pöschl et al.*, 2000; *von Kuhlmann et al.*, 2004]. Photolysis schemes within models are also parametrized in a variety of ways, handling absorption and scattering of radiation by clouds and aerosols differently. About half of the models include some aerosol chemistry (Table A1). It is unclear how important the differences in the current models’ chemical schemes are in generating differences in the distributions of key species such as O₃ and OH, and how the schemes contribute to differing sensitivities to emissions

and climate change. Intercomparisons of specific chemical modules [e.g., *Olson et al.*, 1997; *Pöschl et al.*, 2000] are required to address this issue.

[15] The models vary in maturity; most have undergone some previous validation studies, but not always in their current configurations (see Appendix A). The main purpose of this paper is not model validation, rather we have made the general assumption that the models produce reasonable simulations of the key chemical species. We check this by making a comparison with ozonesonde measurements (below). Other publications in this wider ACCENT study more comprehensively validate NO₂ columns [*van Noije et al.*, 2006], CO (*Shindell et al.*, submitted manuscript, 2006), deposition budgets (*Dentener et al.*, submitted manuscript, 2005), and surface ozone (*Ellingsen et al.*, manuscript in preparation, 2006).

3. Description of the Model Experiments

[16] Five model simulations were specified (Table 1): a year 2000 base case (S1), three 2030 emissions cases (S2–S4, driven by the same meteorological data as S1), and a repeat of S2, but driven by a 2030s climate (S5). Simulations performed by individual models are reported in Table 2. Some models performed multiannual simulations; for these models, results were averaged over all years, to reduce the effects of interannual variability. Multiannual simulations are crucial for isolating the impact of climate change (S5–S2), but are less important for assessing the impacts of emissions changes. Two models (STOCHEM_HadAM3 and UM_CAM) performed multiannual simulations for S5 and S2, but just single year simulations for the other cases; where differences are calculated for these models, we compare like with like (i.e., two single year simulations or two multiyear simulations). Spin-ups of at least 3 months were used for all experiments.

3.1. Emissions

[17] Gridded 1° × 1° anthropogenic emissions of NO_x, CO, NMHCs, SO₂ and NH₃ were specified for the year 2000 and three future emissions scenarios; global totals are given in Table 3. To save time spinning up models, and to help constrain the results, we specified global methane mixing ratios across the model domain (Table 3), using results from earlier transient (1990–2030) integrations of STOCHEM_HadAM3 [*Dentener et al.*, 2005; *Stevenson et al.*, 2005], together with Intergovernmental Panel on Climate Change (IPCC) recommendations for A2 [*IPCC*, 2001, Table II.2.2]. Year 2000 (S1) emissions are based on the EDGAR3.2 data set [*Olivier and Berdowski*, 2001]; three 2030 scenarios are S2, IIASA “current legislation” (CLE); S3, IIASA “maximum feasible reductions” (MFR) [*Dentener et al.*, 2005]; and S4, IPCC SRES A2

Table 2. Number of Simulated Years (Excluding Spin-up) Performed by Individual Models^a

Code Letter	Model Name	S1	S2	S3	S4	S5
A	CHASER_CTM	1	1	1	1	–
B	CHASER_GCM	9	9	–	–	9
C	FRSGC/UCI	1	1	1	1	–
D	GEOS-CHEM	1	1	1	1	–
E	GISS	10(5)	10(5)	5	5	10
F	GMI/CCM3	1	1	1	1	–
G	GMI/DAO	1	1	1	1	–
H	GMI/GISS	1	1	1	1	–
I	IASB	1	1	1	1	–
J	LLNL-IMPACT	1	1	1	1	–
K	LMDz/INCA-CTM	1	1	1	1	–
L	LMDz/INCA-GCM	5	5	–	–	5
M	MATCH-MPIC/ECMWF	1	1	1	1	–
N	MATCH-MPIC/NCEP	1	1	1	1	–
O	MOZ2-GFDL	2	2	2	2	–
P	MOZART4	2	2	2	2	2
Q	MOZECH	5	5	–	–	5
R	MOZECH2	5	5	–	–	5
S	p-TOMCAT	1	1	1	1	–
T	STOCHEM-HadAM3	10(1)	10(1)	1	1	6
U	STOCHEM-HadGEM	5	5	5	5	5
V	TM4	1	1	1	1	–
W	TM5	1	1	–	–	–
X	UIO_CTM2	1	1	1	1	–
Y	ULAQ	10	10	10	10	10
Z	UM_CAM	10(1)	1	1	1	10

^aThree models (GISS, STOCHEM_HadAM3, and UM_CAM) performed multiannual simulations to compare with S5 as well as simulations for a smaller number of years to compare with S3 and S4.

[Nakicenovic et al., 2000]. Ship emissions were added to all emissions scenarios, using EDGAR3.2 emissions for 1995 [Olivier and Berdowski, 2001], and assuming 1.5%/year growth to 2030 in all cases (except for S4, where ships were included at year 2000 levels in error; a separate experiment evaluating 2030 ship emissions for S4 is ongoing (Eyring et al., Multi-model simulations of the impact of international shipping on atmospheric chemistry and climate in 2000 and 2030, manuscript in preparation, 2006)). Aircraft NO_x emissions totals (Table 3) and distributions from NASA or ANCAT [Henderson et al., 1999] were recommended. Aircraft NO_x emissions totals for 2030 (Table 3) were based on the IS92a base scenario [Henderson et al., 1999, Table 9–19]. All the 2030 emissions were “harmonized” to the 2000 emissions, by calculating changes in emissions from 2000 to 2030, then adding them to the base case emissions, to avoid minor inconsistencies.

[18] Satellite-derived monthly varying biomass burning gridded (1° × 1°) distributions [van der Werf et al., 2003]

Table 3. Specified Global Annual Anthropogenic Emission Totals for Each Scenario^a

	S1	S2	S3	S4	S5	TAR
NO _x , Tg N	27.8	32.8	13.1	54.6	32.8	33
CO, Tg	470	397	222	761	397	650
NMVOG, Tg	116	114	73	176	114	161
SO ₂ , Tg S	54	57	17	100	57	76
NH ₃ , Tg N	49	65	65	69	65	36
CH ₄ , ppbv	1760	2088	1760	2163	2012	1745

^aBiomass burning emissions did not vary between scenarios. Specified methane mixing ratios are also given; these were fixed throughout the model domain. Ship emissions are included (for S4, ship emissions for 2000 were used in error). Additional aircraft emissions of 0.8 Tg N (S1) and 1.7 Tg N (all 2030 cases) were recommended. Values from IPCC TAR for year 2000 are also shown for rison.

and totals (Table 4) were specified. These values are averages for the time period 1997–2002, and cover all types of fires (wildfires, savannah burning, and some agricultural waste burning). Ecosystem-specific emission factors from *Andreae and Merlet* [2001] are employed. Domestic and industrial uses of biomass as fuel are included in the anthropogenic emissions. Given the lack of information regarding future levels of biomass burning [e.g., Nakicenovic et al., 2000], these values and distributions were used for 2000 and all 2030 scenarios. The SRES A2 scenario anthropogenic emissions include some biomass burning emissions; these were removed [see, e.g., Stevenson et al., 2000] to avoid double counting. Full details of the anthropogenic and biomass burning emissions can be found at (<http://ccupeople.jrc.it/dentener/index.htm>). Other emissions were specified by individual modelers.

[19] Lightning NO_x production in many of the models is directly linked to the distribution of convection; this is probably the most important and most uncertain natural source of NO_x [e.g., Price et al., 1997; Pickering et al., 1998]. Modelers used lightning NO_x emissions in the range 3.7–7.0 Tg(N) yr⁻¹; in the central part of the range suggested by Price et al. [1997] (1–20 Tg(N) yr⁻¹). Soil NO_x emissions also represent an important natural source, augmented by fertilizer application [e.g., Yienger and Levy, 1995]. Modelers used values in the range 5.5–8.0 Tg(N) yr⁻¹.

[20] Biogenic emissions of isoprene represent the largest NMHC source, mainly emitted from tropical forests. One estimate of total annual emission is 503 Tg(C) [Guenther et al., 1995]. As for the treatment of lightning, some models include interactive isoprene emissions. Modelers used values in the range 220–631 TgC/yr. This relatively wide range, combined with differences in isoprene oxidation mechanisms, will contribute to differences in ozone, particularly in the tropics. Some models also emit significant quantities of other biogenic compounds (e.g., MOZ2-GFDL: Terpene 260 TgC/yr; CH₃OH 287 Tg/yr).

[21] Models include NMHC schemes of varying complexity. The speciation of NMHCs in anthropogenic and biomass burning emissions given by Prather et al. [2001, Table 4.7] was recommended, with species not included in the model either ignored or lumped into related species (e.g., higher alkanes were included as butane). Differences

Table 4. Specified Global Biomass Burning and Recommended Natural Emissions Sources^a

	Sources	This Study	IPCC TAR
NO _x , Tg N	biomass burning	10.2	7.1
NO _x , Tg N	soils	7	5.6
NO _x , Tg N	lightning	5	5.0
CO, Tg	biomass burning	507	700
CO, Tg	oceans/vegetation	100	200
NMHC, Tg	biomass burning	31	42
NMHC, Tg	vegetation isoprene	580	249
NMHC, Tg	vegetation terpenes	295	144
SO ₂ , Tg S	biomass burning	1.4	2.2
SO ₂ , Tg S	volcanoes	14.6	9.3
DMS, Tg S	oceans/terrestrial biosphere	20	24
NH ₃ , Tg N	biomass burning	4.9	5.7
NH ₃ , Tg N	oceans	8.3	8.2
NH ₃ , Tg N	soils	2.4	2.4

^aFixed for all scenarios, except in some models for S5, where some natural emissions are linked to climate. Values from IPCC TAR are shown for comparison.

in model NMHC emission magnitudes, speciation, and chemical schemes probably lead to important variations in modeled ozone, because of the variable formation of PAN and other important NO_y reservoir species. Additional natural sources of trace gases were also recommended (Table 4).

[22] Most models added emissions to the lowest model layer; however several sources (e.g., large industrial sources, major wildfires, and aircraft) inject emissions at higher altitudes. All the models included 3-D emissions of aircraft NO_x . Height profiles for different emission sectors were recommended for those models with the capability to add emissions over several layers. Some models (GMI, IASB, TM4, and TM5) added industrial emissions over the height range 100–300 m; these models and four others (GFDL-MOZ2, LLNL-IMPACT, MOZECH and MOZECH2) implemented biomass burning emissions specified in six layers (boundaries at 0, 0.1, 0.5, 1, 2, 3, and 6 km) [Dentener *et al.*, 2006b].

3.2. Climate Change Scenario (S5)

[23] To gauge the impact of climate change on tropospheric composition by 2030, we repeated the midrange emissions case (S2), but changed the underlying climate to one appropriate for 2030. To generate more statistically significant results, multiannual (5–10 years) simulations were performed and averaged, in order to reduce confounding signals originating from interannual climate variability. The methane boundary condition for S5 was reduced relative to S2 (Table 3), based on earlier results from a fully transient simulation over the time period 1990–2030 using the STOCHEM-HadAM3 model [Stevenson *et al.*, 2005]. Methane concentrations are lower when climate change is taken into account because higher temperatures are accompanied by higher humidities and hence higher OH levels. Higher temperatures and OH levels both promote methane oxidation.

[24] All of the GCMs were configured as atmosphere-only models, with prescribed sea surface temperatures (SSTs) providing the lower boundary condition over the oceans. SSTs and sea-ice distributions from an existing simulation of HadCM3 (Hadley Centre Coupled Model, version 3 [Johns *et al.*, 2003]), forced by the IS92a scenario [Leggett *et al.*, 1992; Cox *et al.*, 2000] were used by most models for the 2030 climate. Some models used their own climate simulations under different scenarios (e.g., MOZECH, MOZECH2: B1; STOCHEM_HadGEM: A2). LMDz/INCA-GCM used SSTs from Rayner *et al.* [1996] for year 2000, together with changes to 2030 given by [Dufresne *et al.*, 2002]. The use of a range of climate scenarios for 2030 introduces a range in the magnitude of the applied climate change; another source of difference between GCMs arises from differing climate sensitivities [e.g., Cubasch *et al.*, 2001]. Global annual mean surface warming between 2000 and 2030 varied from 0.31 K (MOZECH2) to 0.95 K (CHASER_GCM). The range of climate change and chemical responses are discussed in more detail below.

4. Results and Discussion

[25] Each model reported 3-D monthly mean ozone mixing ratios, ozone budget terms and methane oxidation fluxes on their native grids. Each model also reported the mass of each grid box, allowing global burdens and fluxes

to be easily computed. The focus of this study was the troposphere; we apply a mask for grid boxes where monthly mean $\text{O}_3 > 150$ ppbv [e.g., Prather *et al.*, 2001], effectively removing regions above the tropopause. We apply a consistent mask for each model across all scenarios, normally using the ozone field from S1 but in a few cases using the maximum grid box value across all scenarios (this method was used for GMI and GEOS-CHEM, as they masked results “online,” and this was needed to create a consistent mask across all scenarios for these models). Previous studies [e.g., Stevenson *et al.*, 2004] have shown that using various tropopause definitions (e.g., a fixed pressure level, the dynamical tropopause, or the chemical tropopause) can result in significant differences for some terms, such as the tropospheric ozone lifetime and burden. These differences hinder comparisons between models. By using a consistent definition for all models we hope to reduce this source of model differences.

[26] Models used a wide variety of vertical coordinate systems and resolutions. Ozone results were converted to a common vertical grid: the 19 hybrid (sigma pressure) levels of the Met. Office HadAM3 model (the native vertical grid of the UM_CAM model); up to 14 of these levels span the troposphere. Results were also interpolated to a common horizontal resolution of $5^\circ \times 5^\circ$. With results on a common grid, ensemble means and standard deviations for each grid box were calculated. Ozone fields on this grid were also used to calculate radiative forcings. For global tropospheric burdens and budgets, model results were masked (as described above) and then summed on their native grids, to avoid the introduction of any minor errors associated with interpolation.

4.1. Ozone Distributions

4.1.1. Base Year 2000 (S1)

[27] Figure 1 shows ensemble means and standard deviations (absolute and percentage) of annually averaged zonal mean and tropospheric column ozone. The ensemble comprises all 26 models (Table 2). Use of an ensemble should improve the robustness of model results, as individual model errors are likely to cancel, whereas the real signal should reinforce [e.g., Cubasch *et al.*, 2001; Pagowski *et al.*, 2005]. The distribution of standard deviations (SDs) indicates where the models are most consistent, and where they are most uncertain. High SDs close to the tropopause (Figure 1b) are unsurprising, as the models will, almost inevitably, place this region of rapid change in ozone mixing ratios at slightly different altitudes. High SDs throughout the polar troposphere (particularly over the Antarctic; Figures 1c and 1f) are probably also related to differences in the tropopause level at these latitudes, and the resultant stratospheric injection of ozone to the troposphere. Perhaps the most interesting aspect of Figures 1c and 1f is the relatively high SDs ($\sim 30\%$) in the tropics compared to relatively low SDs at midlatitudes ($\sim 20\%$). This larger model uncertainty in the tropics perhaps reflects important intermodel differences in convection parametrizations, biogenic isoprene emissions and chemistry, lightning NO_x production, and the treatment of biomass burning emissions [e.g., Peters *et al.*, 2002]. Midlatitudes are less affected by these factors, and are also closer to the majority of emissions sources; however they might be expected to be more

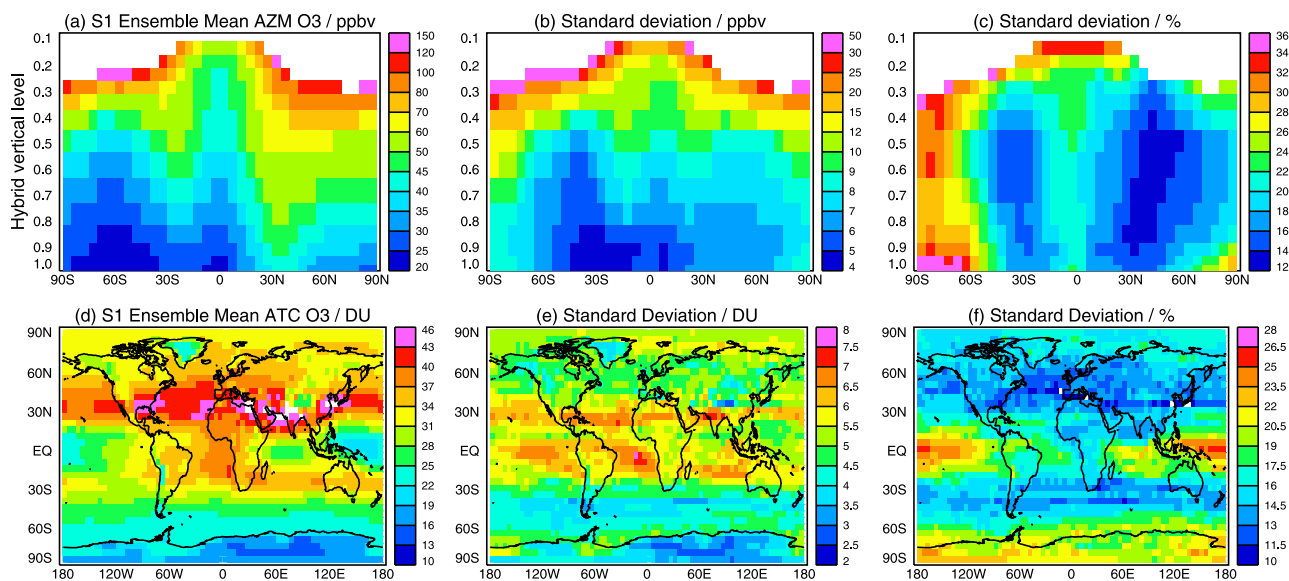


Figure 1. Modeled ozone from case S1 (year 2000): (a–c) zonal annual means (ppbv) and (d–f) tropospheric columns (DU). Figures 1a and 1d are ensemble means (all 26 models); Figures 1b and 1e are absolute standard deviations; Figures 1c and 1f are percentage standard deviations (also known as coefficient of variation). To calculate the ensemble values, individual model results were interpolated to a common grid ($5^\circ \times 5^\circ \times 19$ levels) and masked at the chemical tropopause ($O_3 = 150$ ppbv).

susceptible to uncertainties in stratosphere-troposphere exchange, particularly in the upper troposphere.

[28] The column O_3 plots also show the largest SDs in the tropics, particularly over the oceans. The “step change” in SDs at around $30^\circ\text{N}/30^\circ\text{S}$ (Figure 1e) reflects the latitude of the subtropical jet, where the tropopause shows a discontinuity and jumps to higher levels in the tropics [Highwood and Hoskins, 1998]. Because models place this boundary at slightly different latitudes, this heightens uncertainties in this region. The largest absolute uncertainties are associated with the ozone peak over the tropical South Atlantic (Figure 1e); this peak is seen in observations [e.g., Thompson *et al.*, 2003a, 2003b], and is thought to be associated with the outflow of lightning and biomass burning emissions from Africa. The largest relative uncertainties are for the low-ozone columns over the tropical Pacific (Figure 1f); the large range may relate to model variations in the efficiency of ozone destruction chemistry in comparatively clean environments.

4.1.2. Comparison With Ozonesonde Data

[29] Figure 2 compares the model ensemble mean O_3 for year 2000 with ozonesonde observations, taken from Logan [1999] and Thompson *et al.* [2003a, 2003b]. The Logan data are representative of the time period 1980–1993, while the Thompson *et al.* data are for the years 1997–2002. Although the Logan data do not coincide in time with our simulated year (2000), preliminary analysis of more recent global ozonesonde data reveal only minor trends, suggesting that the earlier data are a useful source for comparison (J. Logan, personal communication, 2005). The Logan [1999] sonde data are located mainly in northern midlatitudes over continental North America, Europe, and Japan, but have been significantly supplemented by the Southern Hemisphere Additional Ozonesondes (SHADOZ) data in the southern tropics [Thompson *et al.* 2003a, 2003b]. The northern

tropics and southern midlatitudes are underrepresented (Figure 2 indicates the number of sites used for each plot).

[30] The comparison indicates that the mean model closely resembles the observations, with the mean values nearly always within a standard deviation of each other. The mean model tends to underestimate the amplitude of the seasonal cycle at 30° – 90°N , overestimating winter ozone by around 10 ppbv. This may reflect the lack of a seasonal cycle in anthropogenic emissions (although it is not obvious that this would improve results), or indicate deficiencies in descriptions of NH stratospheric influx of O_3 . The mean model also tends to slightly overpredict ozone throughout the northern tropics, although this region is only represented by four sites (Naha, Japan; Hilo, Hawaii; Poona, India; and Paramaribo, Suriname). Comparisons in the Southern Hemisphere show good agreement, suggesting that the models’ representation of biomass burning and natural processes (such as lightning and soil emissions) are quite realistic.

[31] Figure 2 also shows results for all individual models (gray lines). These are shown for each model in the auxiliary material.¹ Taking each monthly mean point at each vertical level shown in Figure 2, for each model we calculated a root-mean-square error (RMSE) of the simulated ozone compared to the observed mean. The range in RMSE across all the models is 5.1 to 18.0 ppbv; the mean model has an RMSE of 5.9 ppbv. We later use these RMSE values as part of a criterion for checking the influence of the outlying models on the mean results; models with RMSE values in excess of 12.5 ppbv are considered outliers.

[32] Further validation of ozone precursors is required to increase our confidence in the models’ abilities; NO_2 columns and CO are considered in related papers [van Noije *et al.*, 2006; Shindell *et al.*, submitted manuscript,

¹Auxiliary material is available at <ftp://ftp.agu.org/apend/jd/2005jd006338>.

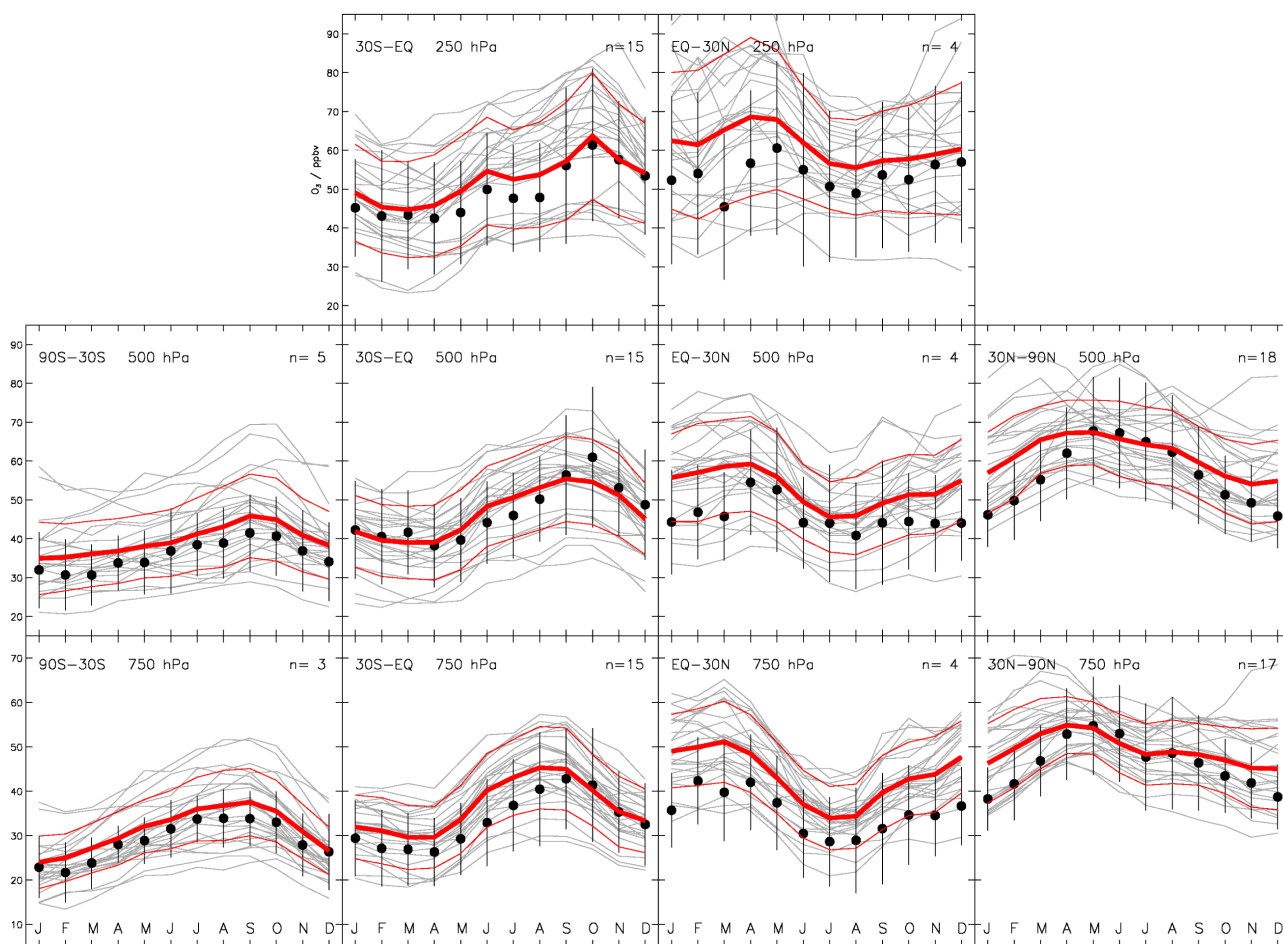


Figure 2. Comparison of the annual cycle of ozone observations (black dots) and model ensemble mean (thick red line), sampled for different latitude bands (90°S – 30°S , 30°S to equator; equator to 30°N , and 30°N – 90°N) and different pressure levels (750, 500, and 250 hPa). The gray lines are the results for each model (also see individual plots in the auxiliary material). Each panel is the mean of several sites (the number of sites is given in the top right corner of each plot); the model and observations are sampled in exactly the same way. The bars for each observation are the average of the interannual standard deviations at each station. The model and observations are the average of the interannual standard deviations at each station. The thin red lines are the standard deviation of the 26 model ensemble. These standard deviations therefore represent different measures of uncertainty, but indicate approximate errors for each point. Data are from Logan [1999] and Thompson *et al.* [2003a, 2003b].

2006]. Validation of hydrocarbons is also highly desirable, but is beyond the scope of this paper. Surface ozone from these simulations is validated in detail by Ellingsen *et al.* (manuscript in preparation, 2006).

4.1.3. Changes 2030–2000 Under Different Emissions Scenarios (S2, S3, and S4)

[33] Figures 3, 4, and 5 present results for the differences in ozone between the three 2030 scenarios (S2, S3 and S4) and the year 2000, following the same format as Figure 1. Under the CLE scenario (S2), ensemble mean ozone shows a zonal annual mean increase of up to 6 ppbv in the northern subtropical upper troposphere (Figure 3a), with an intermodel standard deviation of typically 20–30% (Figure 3c). Changes in column ozone show that the peak increase occurs over India (Figure 3d), reflecting the lack of current legislation limiting ozone precursor emissions in this region.

[34] In the MFR scenario (S3) ozone decreases throughout the troposphere (Fig. 3b), by up to 6 ppbv in the annual

zonal mean, with peak decreases occurring in the lower troposphere at 30° – 40°N . These changes have an associated uncertainty of order 20–30% (similar to those in S2), but there are also significant changes in the upper troposphere with a larger uncertainty of 40–50% (Figure 4c). The larger uncertainties compared to the CLE scenario reflect the more widespread significant changes in emissions (over the entire industrialized world) under this scenario; this experiment therefore samples a wider cross section of model processes. Changes in column ozone (Figure 4d) highlight the industrial regions, with some weighting toward the equator; these locations are those most susceptible to technological reductions in emissions, and hence ozone.

[35] Results for the SRES A2 scenario (S4, Figure 5) remind us of what would happen if we choose to ignore current legislation and allow large growth in ozone precursor emissions; zonal annual mean ozone increases everywhere, typically by 6–10 ppbv in the Northern Hemisphere,

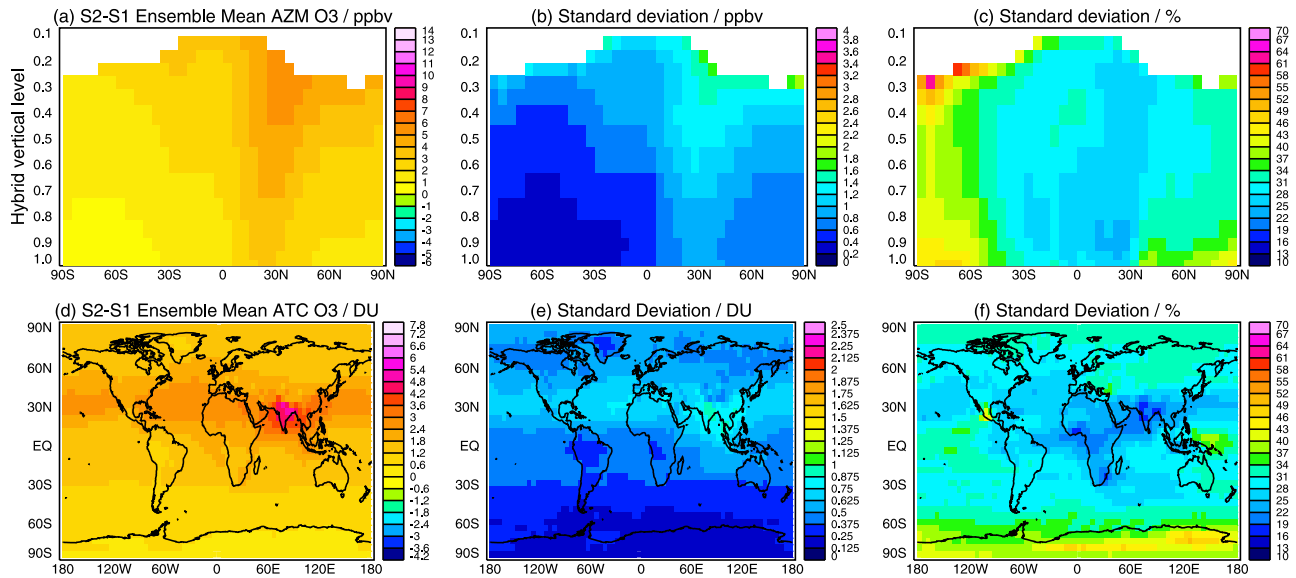


Figure 3. Following the same layout as for Figure 1, the ensemble mean and standard deviation modeled ozone change between case S2 (CLE 2030) and S1 (year 2000). The ensemble comprises all 26 models. Figures 3–5 share the same scales for all panels.

and by up to 13 ppbv in the northern subtropical upper troposphere. The changes have an intermodel uncertainty of around 20–30%, over much of the troposphere (also similar to S2). The column ozone changes show the widespread growth of ozone, particularly in the rapidly developing world (China, southeast Asia, Middle East, plus parts of Africa and Latin America).

[36] The changes in tropospheric ozone burden associated with these three scenarios show a broadly linear relation to changes in NO_x emissions (Figure 6). The emission

changes for scenarios S2–S4 relative to S1 represent changes in total emitted NO_x of +12%, –27% and +55% respectively, and they yield changes in O₃ burden of +6%, –5%, and +15%. A linear relationship should not be expected, partly because of the nonlinearities in O₃ chemistry, but also because of the influence of changes in other trace gas emissions, such as CO, CH₄ and NMHCs [e.g., Wang and Jacob, 1998]. In addition, the relatively meager reduction in ozone under the MFR scenario partly reflects that aircraft emissions show the same growth to 2030 in all

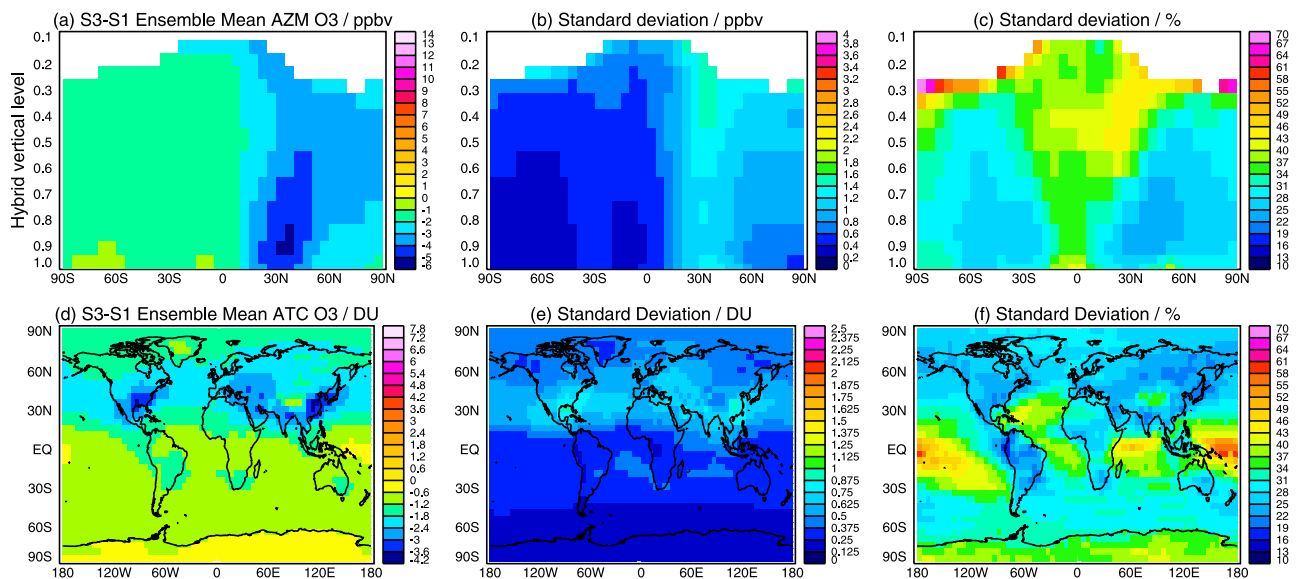


Figure 4. Following the same layout as for Figure 3, the ensemble mean and standard deviation modeled ozone change between case S3 (MFR 2030) and S1 (year 2000). The ensemble comprises the 21 models in Table 2. Figures 3–5 share the same scales for all panels.

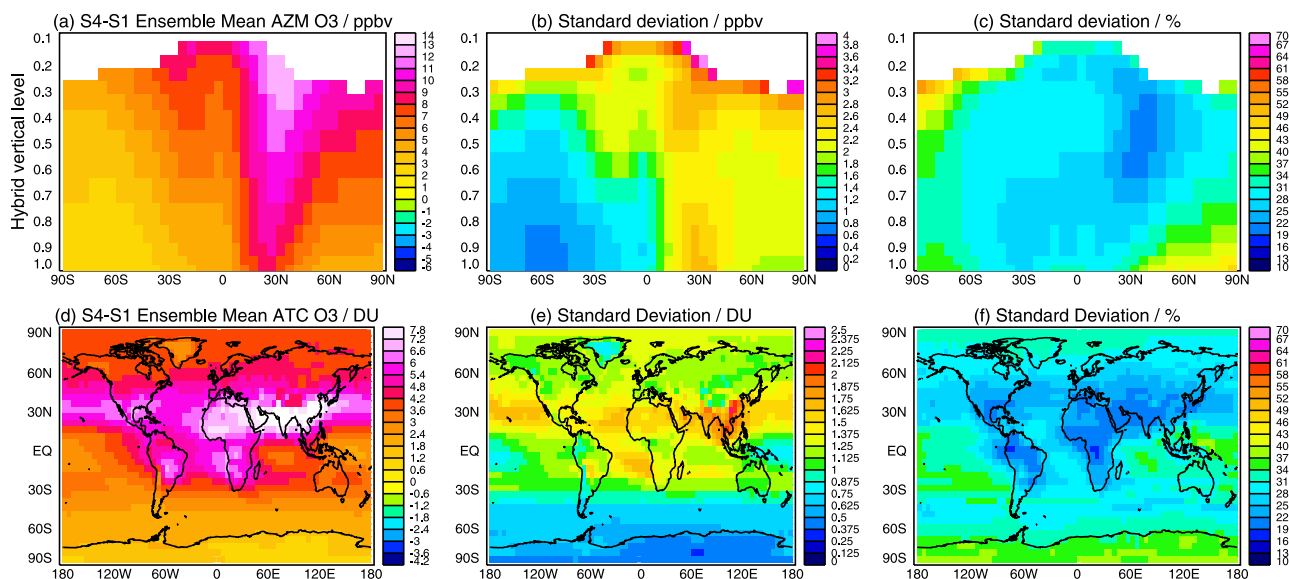


Figure 5. Following the same layout as for Figure 3, the ensemble mean and standard deviation modeled ozone change between case S4 (A2 2030) and S1 (year 2000). The ensemble comprises the 21 models indicated in Table 2. Figures 3–5 share the same scales for all panels.

scenarios, and although the total aircraft emission is small compared to total NO_x , it has a disproportionately large impact, especially as surface emissions are dramatically reduced. This highlights the future problems related to unregulated growth of the aircraft sector, particularly under optimistic scenarios for surface emissions. Ship emissions present similar problems. Nevertheless, Figure 6 provides our best estimate of the overall relationship between changes in global NO_x emissions and tropospheric ozone.

4.1.4. Influence of Climate Change

[37] Figure 7 shows changes in ozone between S5 and S2; Figure 7 follows a slightly different format to Figures 3–5 because the intermodel differences are larger and range between increases and decreases in ozone. For this reason, we plot the ensemble mean (Figures 7b and 7e) together with the mean plus/minus 1 standard deviation, to illustrate the range in results. The mean tropospheric O_3 burden shows a slight decrease related to climate change, with the decrease mainly in the lower troposphere, particularly over the tropical oceans. This negative climate feedback appears to be related to higher humidities and hence increased ozone destruction via reaction (R3) (see section 4.2). At the same time, upper tropospheric ozone rises, especially in the Northern Hemisphere, which is related to an increased influx from the stratosphere. The opposite change occurs in the Southern Hemisphere, owing to a reduced stratospheric influx. These two climate feedbacks (water vapor and stratospheric input) appear to be the dominant mechanisms operating, and different models show variable sensitivities. The two STOCHEM models and GISS are dominated by the water vapor feedback; the other models also tend to show some reductions in tropical lower tropospheric ozone, but are also variably influenced by changes in stratospheric input. We should note that a small reduction in ozone orig from the prescribed change in

methane mixing ratios (Table 3). This prescribed change comes from earlier, transient runs of the STOCHEM_HadAM3 model, over the time period 1990–2030, using very similar emissions scenarios. The response of methane lifetime in this model is, reassuringly, broadly consistent with others, suggesting that fully transient experiments with all models would produce similar results.

4.2. Ozone Budgets

[38] Table 5 gives year 2000 (S1) tropospheric ozone budgets for individual models, together with an ensemble

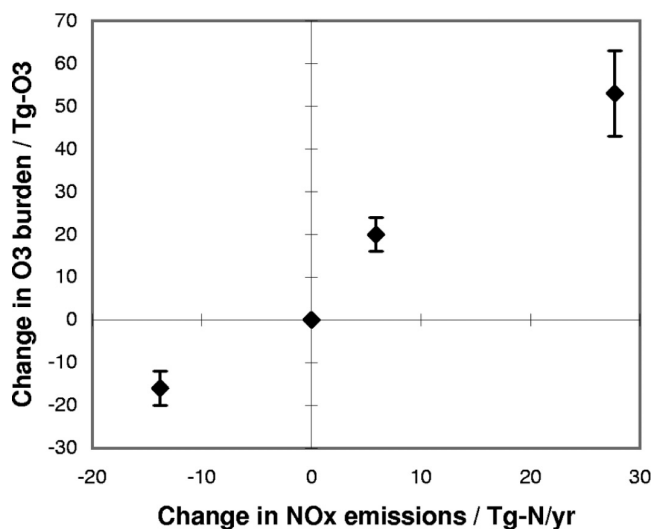


Figure 6. Ensemble mean change in annual mean tropospheric ozone burden versus change in global NO_x emissions for the three scenarios, S2, S3, and S4, relative to S1. The bars represent ± 1 standard deviation within the ensemble members.

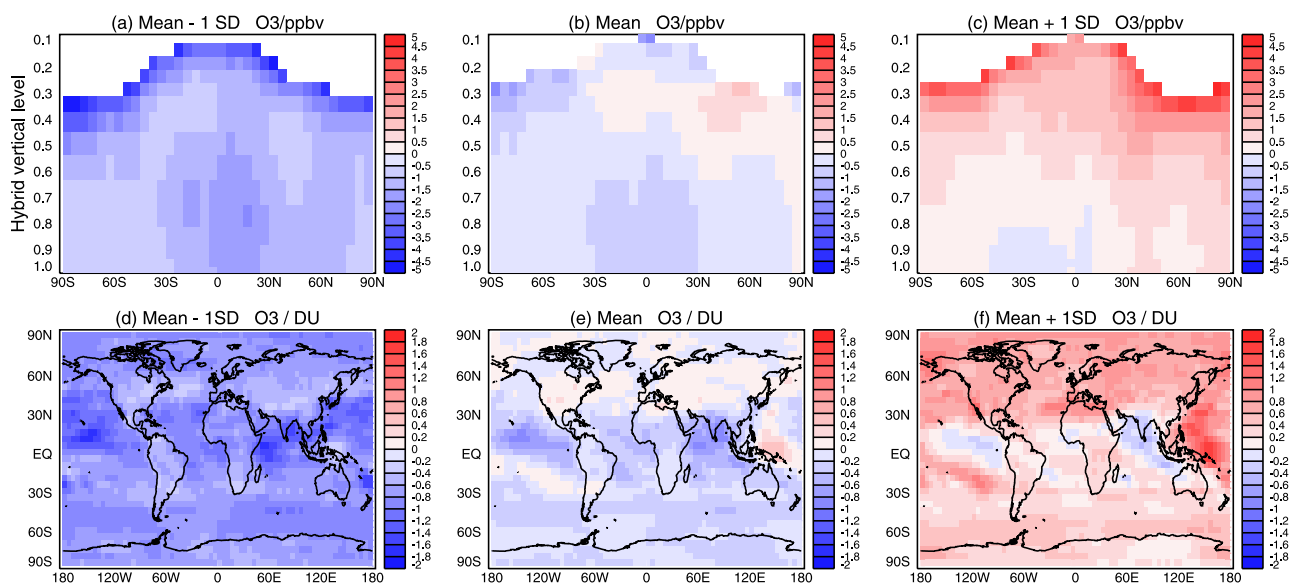


Figure 7. Ozone changes due to climate change: the difference between case S5 (CLE 2030, with a year 2030 climate) and S2 (CLE 2030, with a year 2000 climate). The standard deviations are larger for this case, and the modeled range of ozone change varies in sign. (a and d) Ensemble mean minus 1 standard deviation; (b and e) ensemble mean change; (c and f) ensemble mean plus 1 standard deviation. The ensemble comprises the 10 models indicated in Table 2.

Table 5. Tropospheric O₃ Budget, Burden, Lifetime, and Methane Lifetime for the S1 Simulation for Individual Models^a

	P	L	D	S _{inf}	B _{O₃}	τ _{O₃}	τ _{CH₄}
A. CHASER_CTM	5042	4594	948	501	331	21.8	8.42
B. CHASER_GCM	5032	4620	948	536	333	21.8	8.37
C. FRSGC/UCI	5135	4733	907	505	331	21.4	7.61
D. GEOS-CHEM	<i>4490</i>	<i>3770</i>	<i>1016</i>	<i>296</i>	<i>294</i>	<i>22.4</i>	<i>10.17</i>
E. GISS	—	—	—	—	341	—	8.48
F. GMI/CCM3	5331	5059	862	590	388	23.9	7.50
G. GMI/DAO	5124	4940	763	579	386	24.7	7.64
H. GMI/GISS	4722	4396	856	530	372	25.9	8.54
I. IASB	—	—	—	—	377	—	8.12
J. LLNL-IMPACT	5432	5160	1014	742	406	24.0	7.18
K. LMDz/INCA-CTM	4912	4182	<i>1232</i>	502	330	22.3	8.57
L. LMDz/INCA-GCM	4931	4027	<i>1227</i>	<i>324</i>	316	22.0	8.78
M. MATCH-MPIC/ECMWF	—	—	—	—	377	—	—
N. MATCH-MPIC/NCEP ^a	<i>4342^a</i>	<i>4324^a</i>	<i>948^a</i>	<i>930^a</i>	<i>399</i>	<i>27.9^a</i>	9.48
O. MOZ2-GFDL	5263	5087	963	787	349	21.0	8.42
P. MOZART4	4964	4670	906	612	375	24.5	9.07
Q. MOZECH	<i>6920</i>	<i>6617</i>	963	660	<i>407</i>	<i>19.6</i>	<i>6.31</i>
R. MOZECH2	<i>6130</i>	<i>5876</i>	925	671	387	20.7	7.16
S. p-TOMCAT	—	—	—	—	248	—	<i>12.46</i>
T. STOCHEM-HadAM3	5331	4821	945	435	274	17.3	8.44
U. STOCHEM-HadGEM	5114	<i>3757</i>	<i>1507</i>	<i>151</i>	293	20.3	<i>10.36</i>
V. TM4	4806	4594	720	508	344	23.6	8.80
W. TM5	4580	4623	827	871	339	22.7	7.93
X. UIO_CTM2	—	—	—	—	—	—	<i>10.33</i>
Y. ULAQ	5009	4469	<i>1356</i>	623	328	21.3	8.06
Z. UM_CAM	3922	<i>3363</i>	1172	614	303	24.4	<i>10.57</i>
Mean ± standard deviation (all models)	5110 ± 606	4668 ± 727	1003 ± 200	552 ± 168	344 ± 39	22.3 ± 2.0	8.67 ± 1.32
Mean ± standard deviation (selected models)	4974 ± 223	4577 ± 291	953 ± 154	556 ± 154	336 ± 27	22.2 ± 2.2	8.45 ± 0.38
IPCC TAR	3420	3470	770	770	300	24	8.4

^aP is chemical production, L is chemical loss, D is surface deposition, and S_{inf} is stratospheric input – inferred as the residual of the other terms (all in Tg(O₃) yr⁻¹); B_{O₃} is burden (Tg(O₃)), τ_{O₃} is lifetime (days), and τ_{CH₄} is methane lifetime (years, for the whole atmosphere, assuming a soil sink of 30 Tg yr⁻¹ and a stratospheric sink of 40 Tg yr⁻¹). Models with no O₃ budget terms are not used to calculate the mean values for any of the O₃ terms; budgets for model N were also excluded. Budget terms from model N were calculated using a WMO tropopause definition. Values in italics are > 1 SD above or below the mean value. Mean values are also calculated using a subset of the models, shown in bold (see text for selection criteria). Mean values from IPCC TAR are also given for comparison.

Table 6. Interscenario Ensemble Mean Changes in Tropospheric O₃ Budget Terms, Burden, and Lifetime, and Whole Atmosphere Methane Lifetimes^a

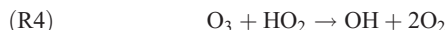
	$\Delta P, \text{Tg(O}_3\text{)yr}^{-1}$	$\Delta L, \text{Tg(O}_3\text{)yr}^{-1}$	$\Delta D, \text{Tg(O}_3\text{)yr}^{-1}$	$\Delta S_{\text{inf}}, \text{Tg(O}_3\text{)yr}^{-1}$	$\Delta B_{\text{O}_3}, \text{Tg(O}_3\text{)}$	$\Delta \tau_{\text{O}_3}, \text{days}$	$\Delta \tau_{\text{CH}_4}, \text{years}$
S2-S1	397 ± 66(7.8%)	325 ± 59(7.0%)	59 ± 16(5.9%)	-11 ± 20(-2.0%)	20 ± 4(5.8%)	-0.19 ± 0.09(-0.9%)	0.23 ± 0.20(2.7%)
S3-S1	-454 ± 70(-8.9%)	-342 ± 47(-7.3%)	-94 ± 28(-9.4%)	18 ± 32(3.3%)	-16 ± 4(-4.7%)	0.76 ± 0.15(3.4%)	0.12 ± 0.18(1.4%)
S4-S1	1205 ± 147(24%)	963 ± 121(21%)	205 ± 54(20%)	-36 ± 75(-6.5%)	53 ± 10(15%)	-1.1 ± 0.2(-4.9%)	0.00 ± 0.31(0.0%)
S5-S2	32 ± 62(0.6%)	87 ± 73(1.7%)	-14 ± 11(-1.3%)	41 ± 31(7.6%)	-1.4 ± 4.2(-0.4%)	-0.34 ± 0.38(-1.5%)	-0.35 ± 0.16(-3.9%)

^aMean is shown ±1 standard deviation, and percentage changes, relative to S1 for S2-S1, S3-S1, and S4-S1 and relative to S2 for S5-S2, are shown in parentheses.

mean and standard deviation. Chemical production (P) is defined as the sum of all the major reactions that convert NO to NO₂:



Chemical loss (L) is dominated by the reactions:



A further small contribution comes from the reactions of O₃ with alkenes and NO_x. Finally, minor net O₃ destruction occurs via a large array of other reactions and processes; we recommended following a scheme whereby net losses of O(^1D), O(^3P), NO₂ or PAN, in addition to O₃, were considered as net ozone losses. In this scheme HNO₃, NO₃ and N₂O₅ are ignored. Some modelers used existing schemes that operated under similar principals; the important point is that fast cycles between ozone-related species are ignored.

[39] Modelers also reported surface deposition fluxes (D). From the three terms, P, L and D, and assuming no tropospheric ozone burden trend (this was confirmed to be negligible in several models), the budget was closed by an inferred stratospheric input term (S_{inf}):

$$S_{\text{inf}} = L + D - P \quad (1)$$

Table 5 also reports tropospheric ozone burdens (B_{O₃}), and lifetimes (τ_{O₃}), defined as

$$\tau_{\text{O}_3} = B_{\text{O}_3}/F_{\text{O}_3} \quad (2)$$

where F_{O₃} is the “ozone turnover flux,” given by

$$F_{\text{O}_3} = L + D (= P + S_{\text{inf}}) \quad (3)$$

Table 5 shows mean P, L, D, and S_{inf} terms of 5110, 4670, 1000 and 550 Tg(O₃) yr⁻¹ respectively, with intermodel standard deviations of 12, 16, 20 and 30%. These can be compared to IPCC T values [Prather *et al.*, 2001,

Table 4.12] (also given in Table 5). It should be noted that the IPCC TAR O₃ budget values represent several independent model studies published between 1996 and 2000, and that these individual studies used a range of emissions, different from those recommended by TAR (reported here in Tables 3 and 4), with total NO_x emissions typically 20% lower than those recommended by TAR. The year 2000 total NO_x emissions recommended by TAR is similar to that used in this study. TAR also recommended isoprene emissions of 220 TgC yr⁻¹, less than half that suggested here (Table 4). The models in TAR Table 4.12 used a wide range of isoprene emissions (some had none), but were generally lower than the emissions used in this study. Table 5 also shows mean B_{O₃} of 340 Tg(O₃) (±11%) and τ_{O₃} of 22 days (±9%); these compare to TAR values of 300 Tg(O₃) (±10%) and 24 days (±8%).

[40] The higher levels of P and L reported here (relative to TAR) are thought to be due to several reasons: (1) higher NO_x emissions, (2) higher isoprene emissions, (3) more detailed NMHC schemes, and possibly (4) improved parametrizations of processes such as photolysis, convection, and stratosphere-troposphere exchange. A series of sensitivity runs were performed with one model (C: FRSGC/UCI), using a variety of anthropogenic NO_x emissions magnitudes and distributions (broadly representative of the pre-TAR simulations reported in TAR Table 4.12), in combination with low/high (220/500 TgC/yr) isoprene emissions. For this model, the change in tropospheric ozone production between that reported in TAR Table 4.12 and that calculated here (Table 5) is an increase of ~20%; with about half of this change due to an increase in NO_x emissions (total NO_x emissions rise by 21%), and the other half due to the increase in isoprene emissions. The year 2000 NO_x emissions used in this study show an equatorward shift compared to data for the 1990s used in earlier studies, and this may also contribute to the increase in P. These sensitivity runs also show a reduction in ozone lifetime of 6% due to the changes in emissions, again with about half from NO_x changes and half from isoprene changes. These largely explain the differences found in the ensemble mean ozone lifetimes between this study and TAR Table 4.12.

[41] The ozone burden has increased by 10% compared to TAR despite a 30% reduction in stratospheric input and a similar increase in dry deposition, and a decrease in the ozone lifetime. Models have clearly increased in chemical activity in the last 5 years.

[42] Table 6 shows absolute and percentage changes in ensemble mean O₃ budget terms between the various 2030 scenarios and 2000, together with standard deviations.

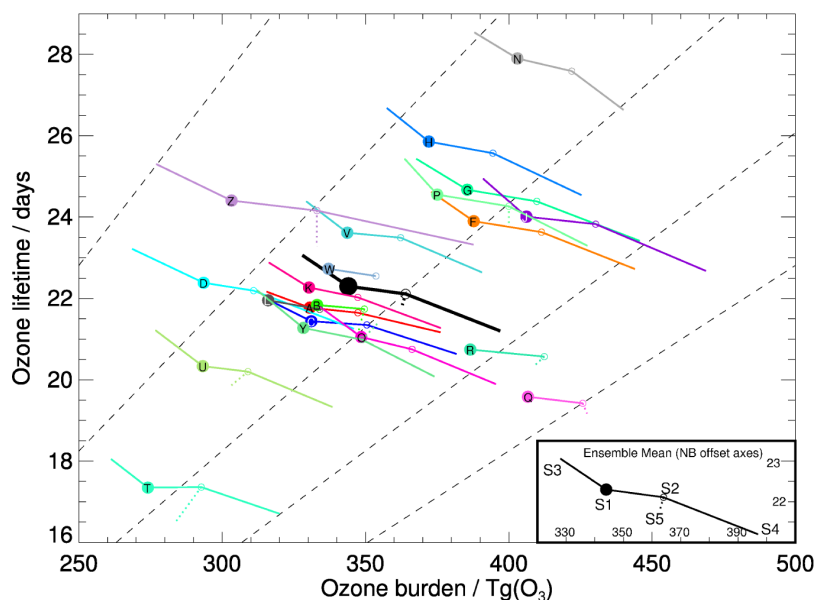
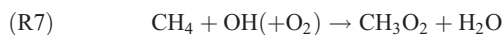


Figure 8. Constellations of ozone lifetime (τ_{O_3} , days) plotted against ozone burden (B_{O_3} , $\text{Tg}(\text{O}_3)$) for individual models. Large solid (small open) circles are values for S1 (S2) for the 21 models that reported ozone budgets (Table 5). The letter refers to the model code (Table 2). Where models reported values for S3 and S4, lines extend to higher and lower burdens, respectively. The nine models that performed S5 and reported budgets are joined by dotted lines to S2 values, the scenario with the same emissions but without climate change. The dashed lines are isolines of overturning flux (F_{O_3}), from $4000 \text{ Tg}(\text{O}_3) \text{ yr}^{-1}$ (top left) to $8000 \text{ Tg}(\text{O}_3) \text{ yr}^{-1}$ (bottom right). Ensemble mean results (Table 6) are plotted oversized in black; the inset shows ensemble mean results, using the same scales but offset axes, labeling the position of each scenario.

Changes in stratospheric influx of ozone are insignificant for all the scenarios with fixed meteorology, as would be expected; however with climate change, this term increases by 8%. The ozone lifetime slightly reduces under S2, while it increases under S3, and quite strongly reduces under S4. These changes occur due to changes in chemical and deposition loss rates. Since water vapor concentrations are fixed in these cases, chemical changes are mainly controlled by reactions (R4) and (R5), and reflect shifts in HO_x amounts and the OH/HO_2 ratio [e.g., *Lelieveld et al.*, 2004]. This ratio is affected by emissions of NO_x , which tends to increase OH , via reaction (R1). Working in the opposite sense, emissions of CO , CH_4 and NMHCs , tend to increase HO_2 , e.g., via the following reactions:



Deposition loss rates change as boundary layer ozone concentrations change; indeed, changes in the 3-D distribution of ozone also affect its overall mean tropospheric lifetime, as the lifetime shows substantial spatial variation.

[43] Climate change tends to further reduce the lifetime, mainly via increases in water vapor, promoting the major ozone loss reaction (R3). However, this is counteracted in some models by increased stratospheric influx, which

increases ozone concentrations in the upper troposphere, where its lifetime is longest.

[44] Figure 8 summarizes all the O_3 budget results on a single diagram, plotting O_3 lifetime against burden, with individual model's results for each scenario linked together. The dashed lines radiating from the origin represent lines of constant turnover flux (equation (3)). There is a clear correlation between models with a long ozone lifetime and high ozone burden, with S1 results congregating around a turnover flux of about $5000\text{--}6000 \text{ Tg}(\text{O}_3) \text{ yr}^{-1}$. There is also a clear tendency for the ozone lifetime to fall as NO_x emissions and the ozone burden increase (i.e., stepping through scenarios in the order S3-S1-S2-S4; see Figure 8, inset) for a given model. The two *STOCHEM* models (especially *STOCHEM-HadAM3*) and *MOZECH* have relatively short ozone lifetimes, while there is a larger grouping with relatively long lifetimes; the root cause of these differences are not obvious. Models with a larger spread between scenarios are more sensitive to changes in emissions; *UM_CAM* is the most sensitive model. The impact of climate change on the ozone budgets for individual models is given in Table 7, and also shown by the dotted lines in Figure 8, which connect the S5 simulation (CLE emissions, 2030 climate) to the same emission scenario simulated with a year 2000 climate (S2). Eight out of nine models show a decrease in ozone lifetime due to climate change. Changes in burden are more variable, but on average show slight decreases (see Figure 8, inset).

Table 7. Background (S2) Tropospheric Water Vapor Burdens (Q) and Differences Between S5 and S2 (Differences due to Climate Change) in Surface Global Annual Mean Temperature (T_0), Q, P, L, D, S_{inf} , B_{O_3} , τ_{O_3} , and τ_{CH_4} for the Subset of Models That Ran S5

Model Letter	Q, Pg-H ₂ O	ΔT_0 , K	ΔQ , Pg-H ₂ O	ΔP , Tg(O ₃)yr ⁻¹	ΔL , Tg(O ₃)yr ⁻¹	ΔD , Tg(O ₃)yr ⁻¹	ΔS_{inf} , Tg(O ₃)yr ⁻¹	ΔB_{O_3} , Tg(O ₃)	$\Delta \tau_{\text{O}_3}$, days	$\Delta \tau_{\text{CH}_4}$, years
B	11.6	0.95	0.68	35	156	-19	101	-2.4	-0.65	-0.46
E	12.5	0.64	0.61	-	-	-	-	-7.1	-	-0.39
L	13.0	0.36	0.38	-5	45	-23	28	0.9	-0.03	-0.29
P	12.1	0.70	0.60	57	122	-13	50	0.0	-0.43	-0.44
Q	13.7	0.33	0.36	99	145	-12	33	1.5	-0.25	-0.28
R	13.4	0.31	0.30	0	30	-12	18	-3.4	-0.22	-0.20
T	13.2	0.66	0.62	122	146	-23	0	-8.7	-0.83	-0.52
U	11.9	0.85	0.95	5	45	-21	19	-6.6	-0.52	-0.64
Y	-	0.52	-	-57	-32	9	34	5.4	0.40	-0.06
Z	13.2 ^a	0.66 ^a	0.62 ^a	75	158	-5	76	-0.1	-0.75	-0.50

^aModel Z (UM_CAM) did not report temperatures or humidities, but it uses the same underlying GCM as model T (STOCHEM_HadAM3), so these values are repeated.

4.3. Methane Lifetimes

[45] Tables 5 and 6 also show whole atmosphere methane lifetimes (τ_{CH_4}). The major methane sink is oxidation by OH (R7). Modelers reported the mass flux through this reaction throughout their model domains; this was then masked above the chemical tropopause (using exactly the same method as above), to yield an annual mean tropospheric oxidation flux ($F_{\text{CH}_4+\text{OH}}$). The other main loss processes for atmospheric methane are a soil sink (F_{SOIL}) and a stratospheric sink (F_{STRAT}). For these two sinks, we use fixed values of 30 Tg/yr and 40 Tg/yr, respectively, as recommended by Prather *et al.* [2001]. We converted specified methane mixing ratios (Table 3) to burdens (B_{CH_4}) using an atmospheric mass of 5136 Eg. The methane lifetime is then given by

$$\tau_{\text{CH}_4} = B_{\text{CH}_4} / (F_{\text{CH}_4+\text{OH}} + F_{\text{SOIL}} + F_{\text{STRAT}}) \quad (4)$$

The ensemble mean (± 1 SD) methane lifetime for S1 is 8.7 ± 1.3 years (Table 5); this is in good agreement with the value of 8.4 years from TAR [Prather *et al.*, 2001, Table 4.3]. Figure 9 shows a clear relationship between the methane lifetime and ozone chemical loss rate (L); this can be understood in terms of reaction (R3), which is both the major ozone loss process, and the primary source of OH (the major methane loss process). In a similar way to Figure 8, Figure 9 summarizes results for all scenarios and all models, and also shows the ensemble mean values (Tables 5 and 6) in an inset. Most models show similar interscenario changes.

[46] The CLE scenario (S2) leads to a 3% increase in methane lifetime (compared to S1), whereas the MFR (S3) and A2 (S4) scenarios have insignificant effects. Under the 2030 climate change scenario (S5), the lifetime reduces by 4%; this reduction is a consistent finding across all nine models and reflects the higher levels of water vapor in a

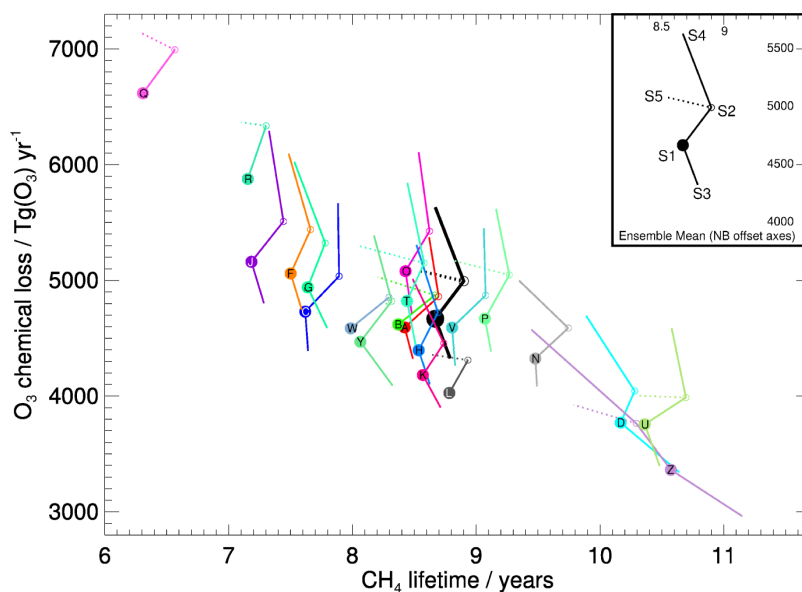


Figure 9. Constellations of tropospheric ozone chemical loss rate (L , Tg(O₃) yr⁻¹) versus methane lifetime (τ_{CH_4} , years) for individual models (S1 data in Table 5), following the same format as Figure 8. Inset shows the ensemble mean results (Table 6), labeling the position of each scenario.

warmer climate, and hence higher levels of OH and methane oxidation (reactions (R3) and (R7)). In addition, reaction (R7) is strongly temperature dependent, with warmer temperatures increasing the oxidation flux. Unlike ozone, there are no other significant climate feedback factors apparent in these simulations, although feedbacks associated with natural emissions (e.g., wetlands) are likely to be significant [e.g., *Gedney et al.*, 2004; *Shindell et al.*, 2004]; these are not included here.

[47] The spread in CH₄ lifetimes (and O₃ chemical loss rates) between models (Figure 9) is not fully understood, but part of the explanation is the underlying level of water vapor, which show some variation between models. Tropospheric water vapor burdens for eight of the GCMs are given in Table 7 and show that the wettest model (Q: MOZECH), also has the shortest CH₄ lifetime, and highest O₃ chemical loss rate (Table 5 and Figure 9). However, amongst the other models there is no clear correlation between high water vapor and these properties. A combination of factors, including both the HO_x sources/sinks, and the OH/HO₂ partitioning must be important – more detailed HO_x budgets are required to further understand these results.

4.4. Ozone and Methane Radiative Forcings 2000–2030

[48] Ozone distributions from all models and all scenarios were inserted into an offline radiation code [*Edwards and Slingo*, 1996], and instantaneous short-wave and long-wave radiative fluxes at the tropopause were calculated. Each ozone distribution was overprinted with a fixed stratospheric ozone distribution above the chemical tropopause, eliminating any effect due to stratospheric ozone changes. Differencing the calculated fluxes between scenarios gives an instantaneous radiative forcing due to the change in tropospheric ozone. The code was set up as described by *Stevenson et al.* [1998], and included the effects of clouds but did not explicitly include stratospheric temperature adjustment. Previous studies with this set up have consistently found a 22% reduction in the instantaneous forcing compared to the equivalent forcing calculated following stratospheric adjustment; we apply this as a constant correction, to make the ozone forcings directly comparable to methane and CO₂ forcings from the same scenarios. Table 8 shows ensemble mean (± 1 SD) tropospheric ozone forcings, together with the equivalent forcings for CH₄ and CO₂. Methane forcings were calculated from the prescribed mixing ratios (Table 3), using the formula from IPCC TAR [*Ramaswamy et al.*, 2001, Table 6.2]; these values do not therefore represent output from this model exercise. Similarly, the CO₂ forcings are taken from IPCC TAR (Table II.3), for the A2 and B2 reference scenarios; CLE and MFR follow the B2 socioeconomic “story line” but impose additional measures to reduce some trace gas emissions (section 3.1); we assume these measures have no effect on CO₂ emissions.

[49] Following the CLE scenario, the combined methane and ozone forcing for the period 2000–2030 adds 23% to the B2 CO₂ forcing (Table 8). In stark contrast, the MFR scenario leads to a negative forcing, equivalent to a 6% reduction of the B2 CO₂ forcing. The higher emission A2 scenario adds 28% to the A2 CO₂ forcing (which is itself 31% larger than the 2 value). By 2030, climate

Table 8. Radiative Forcings Between 2000 and the Three 2030 Scenarios and the Impact of Climate Change on the CLE Scenario in 2030 (S5-S2)^a

	O ₃ , mW m ⁻²	CH ₄ , mW m ⁻²	CH ₄ +O ₃ , mW m ⁻²	CO ₂ , mW m ⁻²
S2-S1	63 ± 15	116	180	780–810 (B2)
S3-S1	-45 ± 15	0	-50	780–810 (B2)
S4-S1	155 ± 37	141	300	1010–1080 (A2)
S5-S2	-3.4 ± 14	-26	-30	-

^aMethane forcings are calculated from the prescribed global mixing ratios given in Table 3, using the formula of *Ramaswamy et al.* [2001, Table 6.2]; they do not therefore reflect the model responses. Carbon dioxide forcings from IPCC [2001, Table II.3] are given for comparison for the appropriate SRES scenario. Given the standard deviations of the ozone forcings, combined forcings are only quoted to the appropriate number of significant figures.

change is estimated to introduce a small negative feedback, about 4% of the B2 CO₂ forcing, mainly via methane. The effect of climate change on ozone, as discussed above, is rather uncertain, and may introduce either a small negative or positive feedback.

4.5. Do Model Outliers Significantly Influence the Results?

[50] The model ensemble comprises a wide range of differently formulated models, and these models simulate present-day ozone to varying degrees of success (Figure 2). The models also exhibit a range of responses to future emissions and climate (Figures 8 and 9), and there are some clear outliers, in terms of their ozone budgets and methane lifetimes. To check if these outliers were significantly biasing the mean model, we selected a subset of models, using two criteria: (1) simulated O₃ has an RMSE less than 12.5 ppbv and (2) methane lifetime is within 1 standard deviation of the mean, i.e., within the range 8.67 ± 1.32 years (Table 5). These criteria selected the subset of models shown in bold in Table 5, which also shows the mean O₃ budget terms and methane lifetime based on this subset of models. The mean values are very similar to the mean of the whole ensemble, indicating that the outliers have little influence on the mean values for the present-day simulation. As would be expected, using this subset reduces the standard deviations of most terms. We also checked if this subset of models produced different results for the various 2030 scenarios, and found that there was no significant influence on the results. We conclude that the outliers have little influence on the mean response, and that use of the entire ensemble represents a robust method for assessing future levels of ozone and quantitatively assessing uncertainties.

5. Summary and Conclusions

[51] This study synthesizes results from a wide range of models (up to 26 different models were used), which collectively represent the best available method for simulating tropospheric composition. Using a model ensemble approach improves the robustness of results, and allows quantification of uncertainties. By considering a range of emission scenarios covering the next thirty years, we have produced quantitative projections of the likely outcomes

from different future regulatory options that are currently open to the world.

[52] Comparison of the ensemble mean model year 2000 simulation with ozonesonde observations (Figure 2) shows good agreement. Column NO_2 distributions from the models also compare well with satellite observations [*van Noije et al.*, 2006]. This suggests that the emissions' specifications and the models' simulation of ozone are consistent with the real atmosphere. The mean model's methane lifetime of 8.7 ± 1.3 years (Table 5) is also in agreement with observationally derived estimates [e.g., *Lawrence et al.*, 2001; *Krol and Lelieveld*, 2003; *Bloss et al.*, 2005; *Bousquet et al.*, 2005; *Prinn et al.*, 2005], indicating that the mean model realistically simulates the global distribution of OH.

[53] The mean model's tropospheric ozone budget for the year 2000 (Table 5) shows distinct differences compared to the budgets reported in IPCC TAR [*Prather et al.*, 2001, Table 4.12]: chemical production is higher by nearly 50%, chemical destruction and dry deposition are larger by 30%, while stratospheric input is 30% less. The mean ozone lifetime is 10% less, while the ozone burden is 10% larger. The reasons for these changes are not immediately obvious, but probably partially relate to the higher total NO_x emissions used here compared to earlier studies; also isoprene emissions are somewhat higher; and NMHC schemes have developed in sophistication over the last 5 years. The sampled models are also different, although a significant subset of the TAR models (and their descendents) is also represented here. The higher value of the simulated present-day ozone burden may lead to a larger estimate of the preindustrial to present-day radiative forcing from tropospheric ozone (although this is not the focus of this study).

[54] Three emission scenarios for the year 2030 were simulated, broadly representing "likely" (S2, CLE), "optimistic" (S3, MFR) and "pessimistic" (S4, A2) future situations. These span global NO_x emission changes, compared to year 2000 (S1), of +12%, -27% and +55% (Table 3) respectively, and yield changes in tropospheric O_3 burden of +6%, -5%, and +15% (Table 6 and Figures 3–6), and net $\text{O}_3 + \text{CH}_4$ radiative forcings for 2000 to 2030 of +180, -50 and +300 mW m^{-2} (Table 8). Simulated changes and forcings have typical intermodel uncertainties (± 1 SD) of 20–35%. These results illustrate the sensitivity of ozone to anthropogenic emissions changes, and hence the degree of human control over this key gas.

[55] A further influence on future tropospheric composition considered here is climate change. By 2030, surface warming on the order of 0.7 K is predicted [*IPCC*, 2001]. Ten of the models performed a climate change simulation (S5), repeating S2 but changing the underlying climate to one appropriate for 2030. This ensemble produced quite divergent results (Table 7) but identified two major feedbacks on ozone that compete for dominance. The first mechanism, apparent to some extent in all the models, involves the increase in water vapor that accompanies warming, which promotes ozone destruction, via reaction (R3). This feedback is strongest in the tropical lower troposphere, particularly over the oceans (Figure 7), and is diagnosed as an increase in chemical loss of ozone (Tables 6 and 7). The second mechanism, apparent in all but one of the models, is an increase in the stratospheric influx of ozone (Tables 6 and 7) leading to increase upper tropo-

spheric ozone, particularly in the Northern Hemisphere. The mean impact of climate change on ozone burden and radiative forcing is a small, but insignificant decrease (Tables 6 and 8).

[56] Climate change has a more consistent impact on methane, increasing its oxidation through both increased levels of OH (also via reaction (R3)), and higher temperatures, which increase the rate coefficient for reaction (R7). The ensemble mean methane lifetime reduces by 4% (Table 6), lowering methane concentrations, and hence radiative forcing (Table 8).

[57] Intermodel standard deviations provide a measure of uncertainty in our ability to simulate ozone. Model simulations of the present-day ozone distribution show the best agreement in the Northern midlatitude midtroposphere (Figure 1c: ± 12 –14%); whereas the models are least consistent throughout the Antarctic troposphere, in the upper troposphere of the Southern Hemisphere and tropics, and in the Arctic lower troposphere ($> \pm 30\%$). Models also show less agreement in the tropics compared to midlatitudes; this probably reflects the larger uncertainties associated with tropical processes such as deep convection, isoprene emissions and chemistry, lightning NO_x , and biomass burning emissions. Northern midlatitudes are the most intensively observed atmospheric region, so we might expect model uncertainties to be lowest here.

[58] We find that model outliers have little influence on the model mean, but, as would be expected, increase intermodel standard deviations, and hence our estimates of model uncertainty. Use of the entire model ensemble gives the best estimate of the mean model response and its uncertainty.

[59] To conclude, this study has shown the extent of anthropogenic control over tropospheric ozone and the oxidizing capacity of the atmosphere, and also the likely effects of climate change over the time period 2000–2030. There are clear benefits to following a trajectory of global emissions reductions, in terms of reducing the radiative forcing of climate, and also for improving air quality (Ellingsen et al., in preparation, 2006) and reducing the environmental impacts from nitrogen and sulphur deposition (Dentener et al., submitted manuscript, 2005). By contrast, the higher emission scenario provides a stark warning of the likely environmental consequences of failing to adhere to current legislation.

[60] All modeling studies have inherent uncertainties; this study uses a large model ensemble approach to reduce and quantify these. In order to reduce these uncertainties, future work will need to focus on the most poorly understood model processes and variables; these include: convection, water vapor, biogenic hydrocarbon emissions and chemistry, natural NO_x emissions, stratosphere-troposphere exchange, and biomass burning.

Appendix A

[61] Table A1 provides a brief summary of information for each of the models, comprising names of the authors responsible for contributing results; model resolution; driving meteorology, including whether the model is a CTM driven by meteorological analyses, or if it is driven by GCM output; details of the convection, advection and tropo-

Table A1. List of Models in Detail

Model	Institute	Contact Author	Resolution Longitude/Latitude/Levels, Top Level	Underlying Meteorology	Advection Scheme	Convection Scheme	Tropospheric Chemistry	Stratospheric Chemistry	GCM Coupling Chemistry to Radiation	References
A. CHASER_CTM	FRCGC/JAMSTEC	Kengo Sudo	2.8°/2.8°/L32, 3 hPa	CTM: ECMWF	<i>Lin and Rood</i> [1996]	Prognostic Anrakawa-Schubert scheme in CCSR/NIES GCM	53 species Interactive SO _x aerosol	O ₃ relaxed above 50 hPa to observations		<i>Sudo et al.</i> [2002a, 2002b, 2003]
B. CHASER_GCM	FRCGC/JAMSTEC	Kengo Sudo	2.8°/2.8°/L32, 3 hPa	GCM: CCSR/NIES	<i>Lin and Rood</i> [1996]	Prognostic Anrakawa-Schubert scheme in CCSR/NIES GCM	53 species Interactive SO _x aerosol	O ₃ relaxed above 50 hPa to observations	Coupled (O ₃ , H ₂ O, N ₂ O, CH ₄ , CFCs)	<i>Sudo et al.</i> [2002a, 2002b, 2003]
FRSGC/UCI	FRCGC/JAMSTEC	Oliver Wild	2.8°/2.8°/L37, 10 hPa	CTM: ECMWF-IFS pieced-forecast data for 2000	<i>Prather</i> [1986]	Mass fluxes taken from ECMWF-IFS fields, based on <i>Tiedtke</i> [1989]	35 species (27 transported), using ASAD [Carver et al., 1997]	LINOZ/ <i>McLinden et al.</i> , 2000		<i>Wild and Prather</i> [2000], <i>Wild et al.</i> [2003]
D. GEOS-CHEM	LMCA-EPFL	Isabelle Bey and Jerome Drevet	5°/4°/L30, 0.01 hPa	CTM: GEOS winds NASA GMAO	<i>Lin and Rood</i> [1996]	Mass fluxes taken from GEOS-3 assimilated fields	31 tracers (24 for O ₃ , 7 for SO _x -NH _x -NO _y aerosols, interactive).	SYNOZ, O ₃ production rate at 70 hPa: 500 Tg/yr [McLinden et al., 2000]		<i>Bey et al.</i> [2001], <i>Martin et al.</i> [2003], <i>Park et al.</i> [2004]
E. GISS	NASA GISS/Columbia University, New York	Nadine Bell and Drew T. Shindell	5°/4°/L23, 0.01 hPa	GCM: ModelE GISS	<i>Prather</i> [1986]	<i>DelGenio et al.</i> [1996]	35 species 20 tracers/interactive SO _x aerosol	O ₃ climatology based on satellite and sonde observations. NO _y set to prescribed NO _x /O ₃ ratios	Decoupled	<i>Shindell et al.</i> [2003, 2005], <i>Bell et al.</i> [2005], <i>Schmidt et al.</i> [2006]
F. GMI/CCM3	NASA Global Modeling Initiative	Jose M. Rodriguez and Susan Strahan	5°/4°/L52, 0.006 hPa	GCM: NCAR MACCM3	<i>Lin and Rood</i> [1996]	Mass fluxes taken from CCM3 deep convection	85 species Off-line SO _x aerosol	O ₃ influx from SYNOZ: 550 Tg/yr		<i>Rotman et al.</i> [2001], <i>Wild et al.</i> [2000], <i>Bey et al.</i> [2001]
G. GMI/DAO	NASA Global Modeling Initiative	Jose M. Rodriguez and Susan Strahan	5°/4°/L46, 0.048 hPa	CTM: GEOS-2-DAS Assimilated fields for Mar 1997–Feb 1998.	<i>Lin and Rood</i> [1996]	Mass fluxes taken from GEOS-2 assimilated fields	85 species Off-line SO _x aerosol	O ₃ influx from SYNOZ: 550 Tg/yr		<i>Rotman et al.</i> [2001], <i>Wild et al.</i> [2000], <i>Bey et al.</i> [2001]
H. GMI/GISS	NASA Global Modeling Initiative	Jose M. Rodriguez and Susan Strahan	5°/4°/L23 0.017 hPa	GCM: GISS-2 ^o	<i>Lin and Rood</i> [1996]	Mass fluxes for deep/shallow convection from GISS-II ^o , as corrected by M. J. Prather (private communication, 2004)	85 species Off-line SO _x aerosol	O ₃ influx from SYNOZ: 550 Tg/yr		<i>Rotman et al.</i> [2001], <i>Wild et al.</i> [2000], <i>Bey et al.</i> [2001]
I. IASB	IASB/Belgium	Jean-Francois Müller	5°/5°/L25, 50 hPa	CTM: Monthly means from ECMWF reanalyses (1993–2001 ERA40)	<i>Smolarkiewicz and Rasch</i> [1991]	Costen et al. [1998]; cumulonimbus distribution taken from ISCCP	60 species (40 transported) Interactive SO _x aerosol	Zonal mean O ₃ prescribed above 98 hPa, zonal mean HNO ₃ prescribed above 50 hPa		<i>Miller and Brasseur</i> [1995], <i>Müller and Stavrakou</i> [2005]
J. LLNL-IMPACT	Lawrence Livermore National Laboratory	Cynthia S. Atherton and Daniel J. Bergmann	5°/4°/L26 2 hPa	GCM: CAM3	<i>Lin and Rood</i> [1996]	<i>Zhang and McFarlane</i> [1995] (deep) and <i>Hack</i> [1994] (shallow)	100 species Including Cl _x , Br _y	Full stratospheric chemistry, including Cl _x , Br _y	Decoupled	<i>Rotman et al.</i> [2004]
K. LMDz/INCA-CTM	LSCE	Didier Hauglustaine and Sophie Szopa	3.75°/2.5°/L19, 3hPa	CTM: nudged to ECMWF/ERA15-ERA40-OD	<i>van Leer</i> [1977]	<i>Tiedtke</i> [1989]	85 species	Stratospheric O ₃ nudged toward climatology above 380 K		<i>Sadourny and Laval</i> [1984], <i>Hauglustaine et al.</i> [2004]
L. LMDz/INCA-GCM	LSCE	Didier Hauglustaine and Sophie Szopa	3.75°/2.5°/L19 3hPa	GCM: LMDz	<i>van Leer</i> [1977]	<i>Tiedtke</i> [1989]	85 species	Stratospheric O ₃ nudged toward climatology above 380 K	Decoupled	<i>Sadourny and Laval</i> [1984], <i>Hauglustaine et al.</i> [2004]

Table A1. (continued)

Model	Institute	Contact Author	Resolution		Underlying Meteorology	Advection Scheme	Convection Scheme	Tropospheric Chemistry	Stratospheric Chemistry	GCM Coupling Chemistry, to Radiation	References
			Longitude/Latitude/Levels, Top Level	Resolution							
M. MATCH-MPIC/ECMWF	Max Planck Institute for Chemistry/NCAR	Tim Butler and Mark Lawrence	5.6°/5.6°/L60, 0.1 hPa		CTM:ECMWF reanalysis	<i>Rasch and Lawrence</i> [1998]	<i>Zhang and McFarlane</i> [1995] (deep) and <i>Hack</i> [1994] (shallow)	60 species	Zonal mean O ₃ climatology above 30 hPa above the tropopause; NO _x set to prescribed NO _x /O ₃ ratios		<i>von Kuhlmann et al.</i> [2003a, 2003b], <i>Lawrence et al.</i> [1999], <i>Rasch et al.</i> [1997]
N. MATCH-MPIC/NCEP	Max Planck Institute for Chemistry/NCAR	Tim Butler and Mark Lawrence	5.6°/5.6°/L60, 0.1 hPa		CTM:NCEP/NCAR reanalysis	<i>Rasch and Lawrence</i> [1998]	<i>Zhang and McFarlane</i> [1995] (deep) and <i>Hack</i> [1994] (shallow)	60 species	Zonal mean O ₃ climatology above 30 hPa above the tropopause; NO _x set to prescribed		<i>von Kuhlmann et al.</i> [2003a, 2003b], <i>Lawrence et al.</i> [1999], <i>Rasch et al.</i> [1997]
O. MOZZ-GFDL	GFDL	Ariane Fiore and Larry Horowitz	1.9°/1.9°/L28, 0.7 hPa		CTM: NCEP reanalysis	<i>Lin and Rood</i> [1996]	<i>Zhang and McFarlane</i> [1995] (deep) and <i>Hack</i> [1994] (shallow)	74 species Interactive SO _x , BC aerosols	Overwrite O ₃ above 14 hPa; between 14 hPa and tropopause relax to climatology (10 day time constant). Relaxed to <i>Legan</i> [1999] above tropopause; above 100 hPa		<i>Brasseur et al.</i> [1998], <i>Hauglustaine et al.</i> [1998], <i>Horowitz et al.</i> [2003]
P. MOZART4	NCAR	Jean Francois Lamarque	2.8°/2.8°/L26, 4 hPa		GCM:CCSM3	<i>Lin and Rood</i> [1996]	<i>Zhang and McFarlane</i> [1995] (deep) and <i>Hack</i> [1994] (shallow)	96 species SO _x , NH ₃ , NO _x , BCOC, seasalt, SOA.	Relaxed to climatology (10 day time constant). Relaxed to stratospheric O ₃ , NO _x , and HNO ₃ down to 200 hPa in extra-tropics and 100 hPa in tropics (10 day time constant)	Decoupled	<i>Horowitz et al.</i> [2003], <i>Tie et al.</i> [2005], <i>Lamarque et al.</i> [2003a, 2003b], <i>Enmons et al.</i> [manuscript in preparation, 2006], <i>S. Rast et al.</i> [manuscript in preparation, 2006], <i>ECHAM5</i> described by <i>Röchner et al.</i> [2003], <i>MOZART-2</i> described by <i>Horowitz et al.</i> [2003]
Q. MOZECH	MPI Meteorology	Martin G. Schultz and Sebastian Rast	1.9°/1.9°/L31, 10 hPa		GCM: ECHAM5	<i>Lin and Rood</i> [1996]	<i>Tiedtke</i> [1989] with modifications after <i>Nordeng</i> [1994]	63 species SO _x climatology	Relaxed to stratospheric O ₃ , NO _x , and HNO ₃ down to 200 hPa in extra-tropics and 100 hPa in tropics (10 day time constant)	Decoupled	<i>Rast et al.</i> [manuscript in preparation], <i>ECHAM5</i> described by <i>Röchner et al.</i> [2003], <i>MOZART-2</i> described by <i>Horowitz et al.</i> [2003]
R. MOZECH2	MPI Meteorology	Martin G. Schultz and Sebastian Rast	2.9°/2.9°/L31, 10 hPa		GCM: ECHAM5	<i>Lin and Rood</i> [1996]	<i>Tiedtke</i> [1989] with modifications after <i>Nordeng</i> [1994]	As MOZECH, but: Lightning NOx reduced to 3.7 Tg N yr ⁻¹ H ₂ O vapor > 700 hPa reduced by 10% in chemistrySurface albedo from <i>Laepple et al.</i> [2005]	Relaxed to stratospheric O ₃ , NO _x , and HNO ₃ down to 200 hPa in extra-tropics and 100 hPa in tropics (10 day time constant)	Decoupled	<i>Rast et al.</i> [manuscript in preparation], <i>ECHAM5</i> described by <i>Röchner et al.</i> [2003], <i>MOZART-2</i> described by <i>Horowitz et al.</i> [2003]
S. p-TOMCAT	University of Cambridge, UK	Nick Savage and John A. Pyle	2.8°/2.8°/L31, 10 hPa		CTM:ECMWF Operational analysis data	<i>Prather</i> [1986]	<i>Tiedtke</i> [1989]	37 species (24 transported) No aerosol	O ₃ fixed above 10 hPa based on 2D model		<i>Law et al.</i> [1998, 2000]
T. STOCHEM-HadAM3	University of Edinburgh	David Stevenson and Ruth Doherty	5°/5°/L9 100 hPa		GCM:HadAM3 vnd4.5	<i>Collins et al.</i> [1997]	<i>Collins et al.</i> [2002]	70 species SO _x -NO _x -NH _x aerosols; interactive	Prescribed O ₃ concentration gradient at 100 hPa	Decoupled	<i>Collins et al.</i> [1997], <i>Stevenson et al.</i> [2004]
U. STOCHEM-HadGEM	UK Met Office	Michael Sanderson and Bill Collins	3.75°/2.5°/L20, 40 km		GCM:HadGEM	<i>Collins et al.</i> [1997]	<i>Collins et al.</i> [2002]	70 species SO _x -NO _x -NH _x aerosols; interactive	Relaxed toward SPARC O ₃ climatology above tropopause	Decoupled	<i>Collins et al.</i> [1997, 2003]

Table A1. (continued)

Model	Institute	Contact Author	Resolution Longitude/Latitude/Levels, Top Level	Underlying Meteorology	Advection Scheme	Convection Scheme	Tropospheric Chemistry	Stratospheric Chemistry	GCM Coupling Chemistry to Radiation	References
V. TM4	KNMI	Twan van Noije	3°/2°/L25, 0.48 hPa	CTM: ECMWF 3-6-h operational forecasts (2000)	Russel and Lerner [1981]	Tiedtke [1989]	37 species (22 transported) SO _x -NO _y -NH _x aerosols, interactive	O ₃ nudged toward climatology above 123 hPa; except 30N–30S, above 60 hPa		Dentener et al. [2003], van Noije et al. [2004]
W. TM5	JRC	Frank Dentener and Maarten Krol	6°/4°/L25, 0.48 hPa (1°/1° Europe, North America, and Asia)	CTM: ECMWF 3-6-h operational forecasts (2000)	Russel and Lerner [1981]	Tiedtke [1989]	37 species (22 transported) SO _x -NO _y -NH _x aerosols, interactive	O ₃ nudged toward climatology above 50 hPa		Dentener et al. [2003], Krol et al. [2005]
Y. ULAQ	University of L'Aquila	Kjerstin Ellingsen and Michael Gauss	2.8°/2.8°/L40, 10 hPa	CTM: ECMWF-IFS forecast data	Prather [1986]	Tiedtke [1989]	58 species	O ₃ , HNO ₃ , and NO _x from OsloCTM2 model run with stratospheric chemistry		Stander [1997]
Z. UM_CAM	University of Cambridge	Veronica Montanaro and Giovanni Pitari	22.5°/10°/L26, 0.04 hPa	GCM: ULAQ-GCM	Eulerian flux form	Pitari et al. [2002] following Miller and Brasseur [1995]	Includes tropospheric aerosols	Detailed stratospheric chemistry scheme, including stratospheric aerosols	Coupled (CO ₂ , H ₂ O, CH ₄ , O ₃ , N ₂ O, CFCs, HCFCs, aerosols)	Pitari et al. [2002]
		Guang Zeng and John Pyle	3.75°/2.5°/L19, 4.6 hPa	GCM: HadAM3 v4.5	Leonard et al. [1995]	Rowntree [1990]	60 species (36 transported) No aerosols.	O ₃ and NO _x prescribed above 30 hPa (Tropospheric chemistry operates below 30 hPa)	Decoupled	Zeng and Pyle [2003, 2005]

spheric/stratospheric chemical schemes; details of any coupling between chemistry and radiation schemes in the GCM-based models; and finally a list of references giving a more detailed model description.

[62] **Acknowledgments.** The EU ACCENT project financed the coordination of this study through support for a workshop in Oslo (January 2005), a Web site (<http://www.accent-network.org>), and a central data repository, managed by Jostein Sundet (University of Oslo). The lead author thanks the Natural Environment Research Council (NERC) and the Environment Agency for fellowship support (NER/J/S/2000/00840, P4-F02).

References

- Andreae, M. O., and P. Merlet (2001), Emission of trace gases and aerosols from biomass burning, *Global Biogeochem. Cycles*, *15*, 955–966.
- Atkinson, R. (2000), Atmospheric chemistry of VOCs and NO_x, *Atmos. Environ.*, *34*, 2063–2101.
- Bauer, S., Y. Balkanski, M. Schulz, D. A. Hauglustaine, and F. Dentener (2004), Heterogeneous chemistry on mineral aerosol surfaces: A global modelling study on the influence on tropospheric ozone chemistry and comparison to observations, *J. Geophys. Res.*, *109*, D02304, doi:10.1029/2003JD003868.
- Bell, N., D. Koch, and D. T. Shindell (2005), Impacts of chemistry-aerosol coupling on tropospheric ozone and sulfate simulations in a general circulation model, *J. Geophys. Res.*, *110*, D14305, doi:10.1029/2004JD005538.
- Bey, I., et al. (2001), Global modelling of tropospheric chemistry with assimilated meteorology: Model description and evaluation, *J. Geophys. Res.*, *106*, 23,073–23,095.
- Bloss, W. J., M. J. Evans, J. D. Lee, R. Sommariva, D. E. Heard, and M. J. Pilling (2005), The oxidative capacity of the troposphere: Coupling of field measurements of OH and a global chemistry transport model, *Faraday Discuss.*, *130*, 425–436, doi:10.1039/b419090d.
- Bousquet, P., D. A. Hauglustaine, P. Peylin, C. Carouge, and P. Ciais (2005), Two decades of OH variability as inferred by an inversion of atmospheric transport and chemistry of methyl chloroform, *Atmos. Chem. Phys. Discuss.*, *5*, 1679–1731.
- Brasseur, G. P., D. A. Hauglustaine, S. Walters, P. J. Rasch, J.-F. Müller, C. Granier, and X. X. Tie (1998), MOZART, a global chemical transport model for ozone and related chemical tracers: 1. Model description, *J. Geophys. Res.*, *103*, 28,265–28,289.
- Brunner, D., et al. (2003), An evaluation of the performance of chemistry transport models by comparison with research aircraft observations. Part 1: Concepts and overall model performance, *Atmos. Chem. Phys.*, *3*, 1609–1631.
- Brunner, D., et al. (2005), An evaluation of the performance of chemistry transport models. Part 2: Detailed comparison with two selected campaigns, *Atmos. Chem. Phys.*, *5*, 107–129.
- Carver, G. D., P. D. Brown, and O. Wild (1997), The ASAD atmospheric chemistry integration package and chemical reaction database, *Comput. Phys. Commun.*, *105*, 197–215.
- Collins, W. J., D. S. Stevenson, C. E. Johnson, and R. G. Derwent (1997), Tropospheric ozone in a global-scale three-dimensional Lagrangian model and its response to NO_x emission controls, *J. Atmos. Chem.*, *26*, 223–274.
- Collins, W. J., D. S. Stevenson, C. E. Johnson, and R. G. Derwent (1999), The role of convection in determining the budget of odd hydrogen in the upper troposphere, *J. Geophys. Res.*, *104*, 26,927–26,941.
- Collins, W. J., R. G. Derwent, C. E. Johnson, and D. S. Stevenson (2002), A comparison of two schemes for the convective transport of chemical species in a Lagrangian global chemistry model, *Q. J. R. Meteorol. Soc.*, *128*, 991–1009.
- Collins, W. J., R. G. Derwent, B. Garnier, C. E. Johnson, M. G. Sanderson, and D. S. Stevenson (2003), The effect of stratosphere-troposphere exchange on the future tropospheric ozone trend, *J. Geophys. Res.*, *108*(D12), 8528, doi:10.1029/2002JD002617.
- Costen, R. C., G. M. Tenille, and J. S. Levine (1998), Cloud pumping in a one-dimensional model, *J. Geophys. Res.*, *93*, 15,941–15,944.
- Cox, P. M., R. A. Betts, C. D. Jones, S. A. Spall, and I. J. Totterdell (2000), Amazonian forest dieback under climate-carbon cycle projections for the 21st Century, *Nature*, *408*, 184–187.
- Crutzen, P. J. (1974), Photochemical reactions initiated by and influencing ozone in the unpolluted troposphere, *Tellus*, *26*, 47–57.
- Crutzen, P. J., and P. H. Zimmerman (1991), The changing photochemistry of the troposphere, *Tellus*, *43*, 136–151.
- Cubasch, U., G. A. Meehl, G. J. Boer, R. J. Stouffer, M. Dix, A. Noda, C. A. Senior, S. Raper, and K. S. Yap (2001) Projections of future

- climate change, in *Climate Change 2001: The Scientific Basis, Contribution of Working Group I to the Third Assessment Report of the Intergovernmental Panel on Climate Change*, edited by J. T. Houghton, pp. 525–582, Cambridge Univ. Press, New York.
- DelGenio, A. D., M. S. Yao, W. Kovari, and K. K. W. Lo (1996), A prognostic cloud water parameterization for global models, *J. Clim.*, *9*(2), 270–304.
- Dentener, F., W. Peters, M. Krol, M. van Weele, P. Bergamaschi, and J. Lelieveld (2003), Interannual variability and trend of CH₄ lifetime as a measure for OH changes in the 1979–1993 time period, *J. Geophys. Res.*, *108*(D15), 4442, doi:10.1029/2002JD002916.
- Dentener, F. D., D. S. Stevenson, J. Cofala, R. Mechler, M. Amann, P. Bergamaschi, F. Raes, and R. G. Derwent (2005), Tropospheric methane and ozone in the period 1990–2030: CTM calculations on the role of air pollutant and methane emissions controls, *Atmos. Chem. Phys.*, *5*, 1731–1755.
- Dentener, F., et al. (2006a), The global atmospheric environment for the next generation, *Environ. Sci. Technol.*, in press.
- Dentener, F., et al. (2006b), Emissions of primary aerosol and precursor gases in the years 2000 and 1750 prescribed data-sets for AeroCom, *Atmos. Chem. Phys. Discuss.*, in press.
- Doherty, R. M., D. S. Stevenson, W. J. Collins, and M. G. Sanderson (2005), Influence of convective transport on tropospheric ozone and its precursors in a chemistry-climate model, *Atmos. Chem. Phys. Discuss.*, *5*, 3747–3771.
- Dufresne, J.-L., P. Friedlingstein, M. Berthelot, L. Bopp, P. Ciais, L. Fairhead, H. Le Treut, and P. Monfray (2002), On the magnitude of positive feedback between future climate change and the carbon cycle, *Geophys. Res. Lett.*, *29*(10), 1405, doi:10.1029/2001GL013777.
- Edwards, J. M., and A. Slingo (1996), Studies with a flexible new radiation code: I: Choosing a configuration for a large-scale model, *Q. J. R. Meteorol. Soc.*, *122*, 689–719.
- Emberson, L. D., M. Ashmore, and F. Murray (2003), *Air Pollution Impacts on Crops and Forests: A Global Assessment*, *Air Pollut. Rev.*, vol. 4, 372 pp., Imperial Coll. Press, London.
- Esler, J. G. (2003), An integrated approach to mixing sensitivities in tropospheric chemistry: A basis for the parameterization of subgrid-scale emissions for chemistry transport models, *J. Geophys. Res.*, *108*(D20), 4632, doi:10.1029/2003JD003627.
- Ganzeveld, L. N., J. Lelieveld, F. J. Dentener, M. C. Krol, A. J. Bouwman, and G.-J. Roelofs (2002), Global soil-biogenic NO_x emissions and the role of canopy processes, *J. Geophys. Res.*, *107*(D16), 4298, doi:10.1029/2001JD001289.
- Gauss, M., et al. (2003), Radiative forcing in the 21st century due to ozone changes in the troposphere and the lower stratosphere, *J. Geophys. Res.*, *108*(D9), 4292, doi:10.1029/2002JD002624.
- Gauss, M., et al. (2005), Radiative forcing since preindustrial times due to ozone change in the troposphere and the lower stratosphere, *Atmos. Chem. Phys. Discuss.*, *5*, 5751–5807.
- Gedney, N., P. M. Cox, and C. Huntingford (2004), Climate feedback from wetland methane emissions, *Geophys. Res. Lett.*, *31*, L20503, doi:10.1029/2004GL020919.
- Gottelman, A., J. R. Holton, and K. H. Rosenlof (1997), Mass fluxes of O₃, CH₄, N₂O, and CF₂Cl₂ in the lower stratosphere calculated from observational data, *J. Geophys. Res.*, *102*, 19,149–19,159.
- Gregory, D., and P. R. Rowntree (1990), A mass flux convection scheme with representation of cloud ensemble characteristics and stability dependent closure, *Mon. Weather Rev.*, *118*, 1483–1506.
- Grenfell, J. L., D. T. Shindell, and V. Grewe (2003), Sensitivity studies of oxidative changes in the troposphere in 2100 using the GISS GCM, *Atmos. Chem. Phys.*, *3*, 1267–1283.
- Guenther, A., et al. (1995), A global model of natural organic compound emissions, *J. Geophys. Res.*, *100*, 8873–8892.
- Hack, J. J. (1994), Parameterization of moist convection in the NCAR community climate model (CCM2), *J. Geophys. Res.*, *99*, 5551–5568.
- Hauglustaine, D. A., G. P. Brasseur, S. Walters, P. J. Rasch, J.-F. Müller, L. K. Emmons, and M. A. Carroll (1998), MOZART, a global chemical transport model for ozone and related chemical tracers: 2. Model results and evaluation, *J. Geophys. Res.*, *103*, 28,291–28,335.
- Hauglustaine, D. A., F. Hourdin, S. Walters, L. Jourdain, M.-A. Filiberti, J.-F. Lamarque, and E. A. Holland (2004), Interactive chemistry in the Laboratoire de Météorologie Dynamique general circulation model: Description and background tropospheric chemistry evaluation, *J. Geophys. Res.*, *109*, D04314, doi:10.1029/2003JD003957.
- Hauglustaine, D. A., J. Lathière, S. Szopa, and G. A. Folberth (2005), Future tropospheric ozone simulated with a climate-chemistry-biosphere model, *Geophys. Res. Lett.*, *32*, L24807, doi:10.1029/2005GL024031.
- Henderson, S. C., et al. (1999), Aircraft emissions: Current inventories and future scenarios, in *IPCC Special Report: Aviation and the Global Atmosphere*, edited by J. E. Penner et al., pp. 290–331, Cambridge Univ. Press, New York.
- Highwood, E. J., and B. J. Hoskins (1998), The tropical tropopause, *Q. J. R. Meteorol. Soc.*, *124*, 1579–1604.
- Horowitz, L. W., et al. (2003), A global simulation of tropospheric ozone and related tracers: Description and evaluation of MOZART, version 2, *J. Geophys. Res.*, *108*(D24), 4784, doi:10.1029/2002JD002853.
- Houweling, S., F. Dentener, and J. Lelieveld (1998), The impact of non-methane hydrocarbon compounds on tropospheric photochemistry, *J. Geophys. Res.*, *103*, 10,673–10,696.
- Intergovernmental Panel on Climate Change (IPCC) (2001), *Climate Change 2001: The Scientific Basis, Contribution of Working Group I to the Third Assessment Report of the Intergovernmental Panel on Climate Change*, edited by J. T. Houghton et al., Cambridge Univ. Press, New York.
- Isaksen, I. S. A., et al. (2003), Ozone-climate interactions, *Air Pollut. Rep.* *81*, 143 pp., Eur. Comm., Brussels.
- Jacob, D. J., et al. (1997), Evaluation and intercomparison of global atmospheric transport models using Rn-222 and other short-lived tracers, *J. Geophys. Res.*, *102*, 5953–5970.
- Johns, T. C., et al. (2003), Anthropogenic climate change for 1860 to 2100 simulated with the HadCM3 model under updated emissions scenarios, *Clim. Dyn.*, *20*, 583–612, doi:10.1007/s00382-002-0296-y.
- Johnson, C. E., W. J. Collins, D. S. Stevenson, and R. G. Derwent (1999), The relative roles of climate and emissions changes on future oxidant concentrations, *J. Geophys. Res.*, *104*(D15), 18,631–18,645.
- Johnson, C. E., D. S. Stevenson, W. J. Collins, and R. G. Derwent (2001), Role of climate feedback on methane and ozone studied with a coupled ocean-atmosphere-chemistry model, *Geophys. Res. Lett.*, *28*, 1723–1726.
- Kinne, S., et al. (2005), An AeroCom initial assessment—Optical properties in aerosol component modules of global models, *Atmos. Chem. Phys. Discuss.*, *5*, 8285–8330.
- Krol, M., and J. Lelieveld (2003), Can the variability in tropospheric OH be deduced from measurements of 1, 1, 1-trichloroethane (methyl chloroform)?, *J. Geophys. Res.*, *108*(D3), 4125, doi:10.1029/2002JD002423.
- Krol, M., S. Houweling, B. Bregman, M. van den Broek, A. Segers, P. van Velthoven, W. Peters, F. Dentener, and B. Bergamaschi (2005), The two-way nested global chemistry-transport zoom model TM5: Algorithm and applications, *Atmos. Chem. Phys.*, *5*, 417–432.
- Laeppe, M. G. Schultz, J.-F. Lamarque, S. Madronich, R. E. Shelter, B. L. Lefer, and E. Atlas (2005), Improved albedo formulation for chemistry transport models based on satellite observations and assimilated snow data and its impact on tropospheric chemistry, *J. Geophys. Res.*, *110*, D11308, doi:10.1029/2004JD005463.
- Lamarque, J.-F., P. Hess, L. Emmons, L. Buja, W. Washington, and C. Granier (2005a), Tropospheric ozone evolution between 1890 and 1990, *J. Geophys. Res.*, *110*, D08304, doi:10.1029/2004JD005537.
- Lamarque, J.-F., J. T. Kiehl, P. G. Hess, W. D. Collins, L. K. Emmons, P. Ginoux, C. Luo, and X. X. Tie (2005b), Response of a coupled chemistry-climate model to changes in aerosol emissions: Global impact on the hydrological cycle and the tropospheric burdens of OH, ozone and NO_x, *Geophys. Res. Lett.*, *32*, L16809, doi:10.1029/2005GL023419.
- Lathière, J., D. A. Hauglustaine, N. de Noblet-Ducoudré, G. Krimmer, and G. A. Folberth (2005), Past and future changes in biogenic volatile organic compound emissions simulated with a global dynamic vegetation model, *Geophys. Res. Lett.*, *32*, L20818, doi:10.1029/2005GL024164.
- Law, K. S., P.-H. Plantévin, D. E. Shallcross, H. L. Rogers, J. A. Pyle, C. Grouhel, V. Thouret, and A. Marengo (1998), Evaluation of modeled O₃ using Measurement of Ozone by Airbus In-Service Aircraft (MOZAIC) data, *J. Geophys. Res.*, *103*, 25,721–25,737.
- Law, K. S., P.-H. Plantévin, V. Thouret, A. Marengo, W. A. H. Asman, M. Lawrence, P. J. Crutzen, J.-F. Müller, D. A. Hauglustaine, and M. Kanakidou (2000), Comparison between global chemistry transport model results and Measurement of Ozone by Airbus In-Service Aircraft (MOZAIC) data, *J. Geophys. Res.*, *105*, 1503–1525.
- Lawrence, M. G., P. J. Crutzen, P. J. Rasch, B. E. Eaton, and N. M. Mahowald (1999), A model for studies of tropospheric photochemistry: Description, global distributions, and evaluation, *J. Geophys. Res.*, *104*, 26,245–26,277.
- Lawrence, M. G., P. Jöckel, and R. von Kuhlmann (2001), What does the global mean OH concentration tell us?, *Atmos. Chem. Phys.*, *1*, 37–49.
- Lawrence, M. G., R. von Kuhlmann, M. Salzmann, and P. J. Rasch (2003), The balance of effects of deep convective mixing on tropospheric ozone, *Geophys. Res. Lett.*, *30*(18), 1940, doi:10.1029/2003GL017644.
- Leggett, J., W. J. Pepper, and R. J. Swart (1992), Emissions scenarios for the IPCC: An update, in *Climate Change 1992: The Supplementary Report to the IPCC Scientific Assessment*, pp. 69–96, Cambridge Univ. Press, New York.

- Lelieveld, J., and P. J. Crutzen (1994), Role of deep cloud convection in the ozone budget of the troposphere, *Science*, *264*, 1759–1761.
- Lelieveld, J., and F. J. Dentener (2000), What controls tropospheric ozone?, *J. Geophys. Res.*, *105*(D3), 3531, doi:10.1029/1999JD901011.
- Lelieveld, J., F. J. Dentener, W. Peters, and M. C. Krol (2004), On the role of hydroxyl radicals in the self-cleansing capacity of the troposphere, *Atmos. Chem. Phys.*, *4*, 2337–2344.
- Leonard, B. P., A. P. Lock, and M. K. MacVean (1995), The NIRVANX scheme applied to one-dimensional advection, *Int. J. Numer. Methods Heat Fluid Flow*, *5*, 341–377.
- Levy, H., J. D. Mahlman, W. J. Moxim, and S. C. Liu (1985), Tropospheric ozone: The role of transport, *J. Geophys. Res.*, *90*, 3753–3772.
- Liang, J., and M. Z. Jacobson (2000), Effects of subgrid segregation on ozone production efficiency in a chemical model, *Atmos. Environ.*, *34*, 2975–2982.
- Lin, S.-J., and R. B. Rood (1996), Multidimensional flux-form semi-Lagrangian transport schemes, *Mon. Weather Rev.*, *124*, 2046–2070.
- Liu, S. C., D. Kley, M. McFarland, J. D. Mahlman, and H. Levy (1980), On the origin of tropospheric ozone, *J. Geophys. Res.*, *85*, 7546–7552.
- Logan, J. A. (1999), An analysis of ozonesonde data for the troposphere: Recommendations for testing 3-D models, and development of a gridded climatology for tropospheric ozone, *J. Geophys. Res.*, *104*, 16,115–16,149.
- Martin, R. V., D. J. Jacob, R. M. Yantosca, M. Chin, and P. Ginoux (2003), Global and regional decreases in tropospheric oxidants from photochemical effects of aerosols, *J. Geophys. Res.*, *108*(D3), 4097, doi:10.1029/2002JD002622.
- McLinden, C. A., S. C. Olsen, B. Hannegan, O. Wild, M. J. Prather, and J. Sundet (2000), Stratospheric ozone in 3-D models: A simple chemistry and the cross-tropopause flux, *J. Geophys. Res.*, *105*(D11), 14,653–14,666.
- Müller, J.-F., and G. P. Brasseur (1995), IMAGES: A three-dimensional chemical transport model of the global troposphere, *J. Geophys. Res.*, *100*, 16,445–16,490.
- Müller, J.-F., and T. Stavrou (2005), Inversion of CO and NO_x emissions using the adjoint of the IMAGES model, *Atmos. Chem. Phys. Discuss.*, *4*, 7985–8068.
- Murazaki, K., and P. Hess (2006), How does climate change contribute to surface ozone change over the United States?, *J. Geophys. Res.*, *111*, D05301, doi:10.1029/2005JD005873.
- Nakicenovic, N., et al. (2000), *Special Report on Emissions Scenarios: A Special Report of Working Group III of the Intergovernmental Panel on Climate Change*, 570 pp., Cambridge Univ. Press, New York.
- Nordeng, T. E. (1994), Extended versions of the convective parameterization scheme at ECMWF and their impact on the mean and transient activity of the model in the tropics, *Tech. Memo. 206*, Eur. Cent. Medium-Range Weather Forecasts, Reading, U. K.
- Olivíć, D. J. L., P. F. J. van Velthoven, A. C. M. Beljaars, and H. M. Kelder (2004), Comparison between archived and off-line diagnosed convective mass fluxes in the chemistry transport model TM3, *J. Geophys. Res.*, *109*, D11303, doi:10.1029/2003JD004036.
- Olivier, J. G. J., and J. J. M. Berdowski (2001), Global emissions sources and sinks, in *The Climate System*, edited by J. J. M. Berdowski, R. Guicherit, and B. J. Heij, A.A. Balkema, Brookfield, Vt.
- Olsen, M. A., M. R. Schoeberl, and A. R. Douglass (2004), Stratosphere-troposphere exchange of mass and ozone, *J. Geophys. Res.*, *109*, D24114, doi:10.1029/2004JD005186.
- Olson, J., et al. (1997), Results from the Intergovernmental Panel on Climate Change Photochemical Model Intercomparison (PHOTOCOMP), *J. Geophys. Res.*, *102*, 5979–5991.
- Pagowski, M., et al. (2005), A simple method to improve ensemble-based ozone forecasts, *Geophys. Res. Lett.*, *32*, L07814, doi:10.1029/2004GL022305.
- Park, R. J., D. J. Jacob, B. D. Field, R. M. Yantosca, and M. Chin (2004), Natural and transboundary pollution influences on sulfate-nitrate-ammonium aerosols in the United States: Implications for policy, *J. Geophys. Res.*, *109*, D15204, doi:10.1029/2003JD004473.
- Peters, W., M. Krol, F. Dentener, A. W. Thompson, and J. Lelieveld (2002), Chemistry-transport modeling of the satellite observed distribution of tropical tropospheric ozone, *Atmos. Chem. Phys.*, *2*, 103–120.
- Pickering, K. E., Y. Wang, W.-K. Tao, C. Price, and J.-F. Müller (1998), Vertical distributions of lightning NO_x for use in regional and global chemical transport models, *J. Geophys. Res.*, *103*, 31,203–31,216.
- Pitari, G., E. Mancini, V. Rizzi, and D. T. Shindell (2002), Impact of future climate and emissions changes on stratospheric aerosols and ozone, *J. Atmos. Sci.*, *59*, 414–440.
- Pöschl, U., R. von Kuhlmann, N. Poisson, and P. J. Crutzen (2000), Development and intercomparison of compressed isoprene oxidation mechanisms for global atmospheric modelling, *J. Atmos. Chem.*, *37*, 29–52.
- Prather, M. J. (1986), Numerical advection by conservation of second-order moments, *J. Geophys. Res.*, *91*, 6671–6681.
- Prather, M., et al. (2001), Atmospheric chemistry and greenhouse gases, in *Climate Change 2001: The Scientific Basis, Contribution of Working Group I to the Third Assessment Report of the Intergovernmental Panel on Climate Change*, edited by J. T. Houghton et al., pp. 239–288, Cambridge Univ. Press, New York.
- Prather, M., et al. (2003), Fresh air in the 21st century, *Geophys. Res. Lett.*, *30*(2), 1100, doi:10.1029/2002GL016285.
- Price, C., J. Penner, and M. Prather (1997), NO_x from lightning: 1. Global distribution based on lightning physics, *J. Geophys. Res.*, *102*, 5929–5941.
- Prinn, R. G., et al. (2005), Evidence for variability of atmospheric hydroxyl radicals over the past quarter century, *Geophys. Res. Lett.*, *32*, L07809, doi:10.1029/2004GL022228.
- Ramaswamy, V., O. Boucher, J. Haigh, D. Hauglustaine, J. Haywood, G. Myhre, T. Nakajima, G. Y. Shi, and S. Solomon (2001), Radiative forcing of climate change, in *Climate Change 2001: The Scientific Basis, Contribution of Working Group I to the Third Assessment Report of the Intergovernmental Panel on Climate Change*, edited by J. T. Houghton et al., pp. 349–416, Cambridge Univ. Press, New York.
- Rasch, P. J., and M. G. Lawrence (1998), Recent developments in transport methods at NCAR, edited by B. Machenhauer, in *MPI Workshop on Conservative Transport Schemes, Rep. 265*, pp. 65–75, Max-Planck-Inst. für Meteorol., Hamburg, Germany.
- Rasch, P. J., N. M. Mahowald, and B. E. Eaton (1997), Representations of transport, convection and the hydrologic cycle in chemical transport models: Implications for the modeling of short lived and soluble species, *J. Geophys. Res.*, *102*, 28,127–28,138.
- Rasch, P. J., et al. (2000), A comparison of scavenging and deposition processes in global models: Results from the WCRP Cambridge Workshop of 1995, *Tellus, Ser. B*, *52*, 1025–1056.
- Rayner, N. A., E. B. Horton, D. E. Parker, C. K. Folland, and R. B. Hackett (1996), Version 2.2 of the global sea-ice and sea-surface temperature data set, 1903–1994, CRTN 74, Hadley Centre, Met Off., Bracknell, U.K.
- Robertson, L. B., D. S. Stevenson, and F. Conen (2005), Test of a northwards decreasing ²²²Rn source term by comparison of modeled and observed ²²²Rn concentrations, *Tellus, Ser. B*, *57*, 116–123.
- Röckner, E., et al. (2003), The atmospheric general circulation model ECHAM 5. Part I: Model description, *Rep. 349*, Max Planck Inst. for Meteorol., Hamburg, Germany. (Available at http://mpi-web.dkrz.de/de/web/science/a_reports_archive.php?actual=2003#)
- Roelofs, G.-J., and J. Lelieveld (2000), Tropospheric ozone simulation with a chemistry-general circulation model: Influence of higher hydrocarbon chemistry, *J. Geophys. Res.*, *105*, 22,697–22,712.
- Roelofs, G.-J., et al. (2003), Intercomparison of tropospheric ozone models: Ozone transport in a complex tropopause folding event, *J. Geophys. Res.*, *108*(D12), 8529, doi:10.1029/2003JD003462.
- Rotman, D. A., et al. (2001), Global Modeling Initiative assessment model: Model description, integration, and testing of the transport shell, *J. Geophys. Res.*, *106*, 1669–1691.
- Rotman, D. A., et al. (2004), IMPACT, the LLNL 3-D global atmospheric chemical transport model for the combined troposphere and stratosphere: Model description and analysis of ozone and other trace gases, *J. Geophys. Res.*, *109*, D04303, doi:10.1029/2002JD003155.
- Russell, G. L., and J. A. Lerner (1981), A new finite-differencing scheme for the tracer transport equation, *J. Appl. Meteorol.*, *20*, 1483–1498.
- Sadourny, R., and K. Laval (1984), January and July performance of the LMD general circulation model, in *New Perspectives in Climate Modeling*, edited by A. Berger and C. Nicolis, pp. 173–197, Elsevier, New York.
- Sanderson, M. G., C. D. Jones, W. J. Collins, C. E. Johnson, and R. G. Derwent (2003), Effect of climate change on isoprene emissions and surface ozone levels, *Geophys. Res. Lett.*, *30*(18), 1936, doi:10.1029/2003GL017642.
- Schmidt, G. A., et al. (2006), Present day atmospheric simulations using GISS ModelE: Comparison to in-situ, satellite and reanalysis data, *J. Clim.*, *19*, 153–192, doi:10.1175/JCLI3612.1.
- Shindell, D. T., G. Faluvegi, and N. Bell (2003), Preindustrial-to-present-day radiative forcing by tropospheric ozone from improved simulations with the GISS chemistry-climate GCM, *Atmos. Chem. Phys.*, *3*, 1675–1702.
- Shindell, D. T., B. P. Walter, and G. Faluvegi (2004), Impacts of climate change on methane emissions from wetlands, *Geophys. Res. Lett.*, *31*, L21202, doi:10.1029/2004GL021009.
- Shindell, D. T., G. Faluvegi, N. Bell, and G. A. Schmidt (2005), An emissions-based view of climate forcing by methane and tropospheric ozone, *Geophys. Res. Lett.*, *32*, L04803, doi:10.1029/2004GL021900.

- Simmons, A. J., and J. K. Gibson (2000), The ERA-40 project plan, *ERA-40 Proj. Rep. Ser. Tech. Rep. 1*, Eur. Cent. for Medium-Range Weather Forecasts, Reading, U. K.
- Smolarkiewicz, P., and P. J. Rasch (1991), Monotone advection on the sphere: An Eulerian versus semi-Lagrangian approach, *J. Atmos. Sci.*, **48**, 793–810.
- Stahelin, J., J. Thudium, R. Buehler, A. Volz-Thomas, and W. Graber (1994), Trends in surface ozone concentrations at Arosa (Switzerland), *Atmos. Environ.*, **28**, 75–87.
- Stevenson, D. S., C. E. Johnson, W. J. Collins, R. G. Derwent, K. P. Shine, and J. M. Edwards (1998), Evolution of tropospheric ozone radiative forcing, *Geophys. Res. Lett.*, **25**, 3819–3822.
- Stevenson, D. S., C. E. Johnson, W. J. Collins, R. G. Derwent, and J. M. Edwards (2000), Future tropospheric ozone radiative forcing and methane turnover—The impact of climate change, *Geophys. Res. Lett.*, **27**, 2073–2076.
- Stevenson, D. S., R. M. Doherty, M. G. Sanderson, W. J. Collins, C. E. Johnson, and R. G. Derwent (2004), Radiative forcing from aircraft NO_x emissions: Mechanisms and seasonal dependence, *J. Geophys. Res.*, **109**, D17307, doi:10.1029/2004JD004759.
- Stevenson, D. S., R. M. Doherty, M. G. Sanderson, C. E. Johnson, W. J. Collins, and R. G. Derwent (2005), Impacts of climate change and variability on tropospheric ozone and its precursors, *Faraday Discuss.*, **130**, 41–57, doi:10.1039/b417412g.
- Sudo, K., and M. Takahashi (2001), Simulation of tropospheric ozone changes during the 1997–1998 El Niño: Meteorological impact on tropospheric photochemistry, *Geophys. Res. Lett.*, **28**, 4091–4094.
- Sudo, K., M. Takahashi, J. Kurokawa, and H. Akimoto (2002a), CHASER: A global chemical model of the troposphere: 1. Model description, *J. Geophys. Res.*, **107**(D17), 4339, doi:10.1029/2001JD001113.
- Sudo, K., M. Takahashi, and H. Akimoto (2002b), CHASER: A global chemical model of the troposphere: 2. Model results and evaluation, *J. Geophys. Res.*, **107**(D21), 4586, doi:10.1029/2001JD001114.
- Sudo, K., M. Takahashi, and H. Akimoto (2003), Future changes in stratosphere-troposphere exchange and their impacts on future tropospheric ozone simulations, *Geophys. Res. Lett.*, **30**(24), 2256, doi:10.1029/2003GL018526.
- Sundet, J. K. (1997), Model studies with a 3-D global CTM using ECMWF data, Ph.D. thesis., Dep. of Geophys., Univ. of Oslo, Oslo.
- Textor, C., et al. (2005), Analysis and quantification of the diversities of aerosol life cycles within AeroCom, *Atmos. Chem. Phys. Discuss.*, **5**, 8331–8420.
- Thompson, A. M., et al. (2003a), Southern Hemisphere Additional Ozone-sondes (SHADOZ) 1998–2000 tropical ozone climatology: 1. Comparison with Total Ozone Mapping Spectrometer (TOMS) and ground-based measurements, *J. Geophys. Res.*, **108**(D2), 8238, doi:10.1029/2001JD000967.
- Thompson, A. M., et al. (2003b), Southern Hemisphere Additional Ozone-sondes (SHADOZ) 1998–2000 tropical ozone climatology: 2. Tropospheric variability and the zonal wave-one, *J. Geophys. Res.*, **108**(D2), 8241, doi:10.1029/2002JD002241.
- Tie, X. X., G. Brasseur, L. Emmons, L. Horowitz, and D. Kinnison (2001), Effects of aerosols on tropospheric oxidants: A global model study, *J. Geophys. Res.*, **106**, 22,931–22,964.
- Tie, X. X., L. Emmons, L. Horowitz, G. Brasseur, B. Ridley, E. Atlas, C. Stround, P. Hess, A. Klonecki, S. Madronich, R. Talbot, and J. Dibb (2003), Effect of sulfate aerosol on tropospheric NO_x and ozone budgets: Model simulations and TOPSE evidence, *J. Geophys. Res.*, **108**(D4), 8364, doi:10.1029/2001JD001508.
- Tie, X. X., S. Madronich, S. Walters, D. P. Edwards, P. Ginoux, N. Mahowald, R. Zhang, C. Lou, and G. Brasseur (2005), Assessment of the global impact of aerosols on tropospheric oxidants, *J. Geophys. Res.*, **110**, D03204, doi:10.1029/2004JD005359.
- Tiedtke, M. (1989), A comprehensive mass flux scheme for cumulus parameterization in large-scale models, *Mon. Weather Rev.*, **117**, 1779–1800.
- van der Werf, G. R., T. J. Randerson, J. Collatz, and L. Giglio (2003), Carbon emissions from fires in tropical and subtropical ecosystems, *Global Change Biol.*, **9**, 547–562.
- van Leer, B. (1977), Toward the ultimate conservative difference scheme. Part IV: A new approach to numerical convection, *J. Comput. Phys.*, **23**, 276–299.
- van Noije, T. P. C., H. J. Eskes, M. van Weele, and P. F. J. van Velthoven (2004), Implications of the enhanced Brewer-Dobson circulation in European Centre for Medium-Range Weather Forecasts reanalysis ERA-40 for the stratosphere-troposphere exchange of ozone in global chemistry-transport models, *J. Geophys. Res.*, **109**, D19308, doi:10.1029/2004JD004586.
- van Noije, T. P. C., et al. (2006), Multi-model ensemble simulations of tropospheric NO₂ compared with GOME retrievals for the year 2000, *Atmos. Chem. Phys. Discuss.* in press.
- Volz, A., and D. Kley (1988), Evaluation of the Montsouris series of ozone measurements made in the 19th century, *Nature*, **332**, 240–242.
- von Kuhlmann, R., M. G. Lawrence, P. J. Crutzen, and P. J. Rasch (2003a), A model for studies of tropospheric ozone and nonmethane hydrocarbons: Model description and ozone results, *J. Geophys. Res.*, **108**(D9), 4294, doi:10.1029/2002JD002893.
- von Kuhlmann, R., M. G. Lawrence, P. J. Crutzen, and P. J. Rasch (2003b), A model for studies of tropospheric ozone and nonmethane hydrocarbons: Model evaluation of ozone-related species, *J. Geophys. Res.*, **108**(D23), 4729, doi:10.1029/2002JD003348.
- von Kuhlmann, R., M. G. Lawrence, U. Pöschl, and P. J. Crutzen (2004), Sensitivities in global scale modelling of isoprene, *Atmos. Chem. Phys.*, **4**, 1–17.
- Walter, B. P., and M. Heimann (2000), A process-based, climate-sensitive model to derive methane emissions from natural wetlands: Application to five wetland sites, sensitivity to model parameters, and climate, *Global Biogeochem. Cycles*, **14**, 745–766.
- Wang, X., and D. L. Mauzerall (2004), Characterizing distributions of surface ozone and its impact on grain production in China, Japan, and South Korea, *Atmos. Environ.*, **38**, 4383–4402.
- Wang, Y., and D. J. Jacob (1998), Anthropogenic forcing on tropospheric ozone and OH since preindustrial times, *J. Geophys. Res.*, **103**, 31,123–31,135.
- Wang, Y., D. J. Jacob, and J. A. Logan (1998), Global simulation of tropospheric O₃-NO_x-hydrocarbon chemistry: 3. Origin of tropospheric ozone and effects of nonmethane hydrocarbons, *J. Geophys. Res.*, **103**, 10,757–10,767.
- Wesely, M. L. (1989), Parametrization of surface resistances to gaseous dry deposition in regional-scale numerical models, *Atmos. Environ.*, **23**, 1293–1304.
- Wiedinmyer, C., et al. (2005), Ozarks Isoprene Experiment (OZIE): Measurements and modeling of the “isoprene volcano,” *J. Geophys. Res.*, **110**, D18307, doi:10.1029/2005JD005800.
- Wild, O., and M. J. Prather (2000), Excitation of the primary tropospheric chemical mode in a global 3-D model, *J. Geophys. Res.*, **105**, 24,647–24,660.
- Wild, O., X. Zhu, and M. J. Prather (2000), Fast-j: Accurate simulation of in- and below-cloud photolysis in tropospheric chemical models, *J. Atmos. Chem.*, **37**, 245–282.
- Wild, O., J. K. Sundet, M. J. Prather, I. S. A. Isaksen, H. Akimoto, E. V. Browell, and S. J. Oltmans (2003), CTM ozone simulations for spring 2001 over the western Pacific: Comparisons with TRACE-P Lidar, ozonesondes and TOMS columns, *J. Geophys. Res.*, **108**(D21), 8826, doi:10.1029/2002JD003283.
- World Health Organization (2003), Health aspects of air pollution with particulate matter, ozone, and nitrogen dioxide, *Rep. EUR/03/5042688*, Bonn.
- Yienger, J. J., and H. Levy II (1995), Empirical model of global soil-biogenic NO_x emissions, *J. Geophys. Res.*, **100**, 11,447–11,464.
- Zeng, G., and J. A. Pyle (2003), Changes in tropospheric ozone between 2000 and 2100 modeled in a chemistry-climate model, *Geophys. Res. Lett.*, **30**(7), 1392, doi:10.1029/2002GL016708.
- Zeng, G., and J. A. Pyle (2005), Influence of El Niño Southern Oscillation on stratosphere/troposphere exchange and the global tropospheric ozone budget, *Geophys. Res. Lett.*, **32**, L01814, doi:10.1029/2004GL021353.
- Zhang, G. J., and N. A. McFarlane (1995), Sensitivity of climate simulations to the parameterization of cumulus convection in the Canadian climate centre general circulation model, *Atmos. Ocean*, **33**, 407–446.

M. Amann and J. Cofala, International Institute for Applied Systems Analysis, A-2361 Laxenburg, Austria.

C. S. Atherton and D. J. Bergmann, Atmospheric Science Division, Lawrence Livermore National Laboratory, 7000 East Avenue, Livermore, CA 94550, USA.

N. Bell and D. T. Shindell, NASA Goddard Institute for Space Studies, 2880 Broadway, New York, NY 10025, USA.

I. Bey and J. Drevet, Ecole Polytechnique Fédérale de Lausanne, CH-1015, Lausanne, Switzerland.

T. Butler and M. G. Lawrence, Max Planck Institute for Chemistry, Joh.-Joachim-Becher-Weg 27, D-55128 Mainz, Germany.

W. J. Collins and M. G. Sanderson, Hadley Centre for Climate Prediction and Research, Met Office, FitzRoy Road, Exeter, Devon EX1 3PB, UK.

F. J. Dentener and M. C. Krol, Joint Research Centre, Institute for Environment and Sustainability, Via E. Fermi 1, I-21020 Ispra, Italy.

R. G. Derwent, rdscientific, Newbury, RG14 6LH Berkshire, UK.

R. M. Doherty and D. S. Stevenson, School of Geosciences, University of Edinburgh, Crew Building, King's Buildings, Edinburgh EH9 3J9, UK. (dstevens@staffmail.ed.ac.uk)

K. Ellingsen, M. Gauss, and I. S. A. Isaksen, Department of Geosciences, University of Oslo, Boks 1072 Blindern, NO-0316 Oslo, Norway.

H. J. Eskes and T. P. C. van Noije, Atmospheric Composition Research, KNMI, NL-3730, AE De Bilt, Netherlands.

A. M. Fiore and L. W. Horowitz, GFDL, NOAA, 201 Forrestal Road, Princeton, NJ 08540-6649, USA.

D. A. Hauglustaine and S. Szopa, Laboratoire des Sciences du Climat et de l'Environnement, Orme des Merisiers, Bat. 709, F-91191 Gif-sur-Yvette, France.

J.-F. Lamarque, Atmospheric Chemistry Division, National Center of Atmospheric Research, P.O. Box 3000, Boulder, CO 80307-3000, USA.

V. Montanaro and G. Pitari, Dipartimento di Fisica, Università L'Aquila, I-67010 L'Aquila, Italy.

J.-F. Müller, Belgian Institute for Space Aeronomy, Avenue Circulaire, 3 B-1180 Brussels, Belgium.

M. J. Prather, Department of Earth System Science, University of California, Irvine, CA 92697, USA.

J. A. Pyle, N. H. Savage, O. Wild, and G. Zeng, Centre for Atmospheric Science, University of Cambridge, Cambridge CB2 1EW, UK.

S. Rast and M. G. Schultz, Max Planck Institute for Meteorology, Bundesstraße 53, D-20146 Hamburg, Germany.

J. M. Rodriguez, Rosentiel School of Marine and Atmospheric Sciences, University of Miami, 4600 Rickenbacker Causeway, Miami, FL 33149, USA.

S. E. Strahan, GEST, 5523 Research Park Drive, Suite 320, Baltimore, MD 21228, USA.

K. Sudo, Frontier Research Center for Global Change, JAMSTEC, 3173-25, Showamachi, Kanazawa-Ku, Yokohama, Kanagawa, 236-0001, Japan.